Vesicular acetylcholine transporter (VAChT) over-expression induces major modifications of striatal cholinergic interneuron morphology and function

Helena Janickova, Vania F. Prado, Marco A. M. Prado, Salah El Mestikawy, Véronique Bernard

Vesicular Acetylcholine Transporter (VAChT) overexpression induces major modifications of striatal cholinergic interneuron morphology and function

Helena Janickova[1], Vania F. Prado[1], Marco A.M. Prado[1], Salah El Mestikawy[2,3] and Véronique Bernard[2*]

[1]Robarts Research Institute, Molecular Medicine Laboratories, Department of Physiology and Pharmacology and Department of Anatomy & Cell Biology, The University of Western Ontario, 1151 Richmond St. N, N6A 5B7, London, Ontario, Canada; [2]Sorbonne Universités, Université Pierre et Marie Curie UM 119 - CNRS UMR 8246 - INSERM U1130, Neurosciences Paris Seine - Institut de Biologie Paris Seine (NPS - IBPS), 75005 Paris, France,
[3]Douglas Mental Health University Institute, Department of Psychiatry, McGill University, Montreal, Canada.

* **Corresponding author** : Véronique Bernard, Neuroscience Paris Seine, Sorbonne Universités, Université Pierre et Marie Curie UM 119 - CNRS UMR 8246 - INSERM U1130, Bât B 4ème étage pièce 425, 9 quai Saint Bernard, case courrier 37, 75005, Paris, France,
Tel: +33 6 10 09 68 93; Fax: +33 1 44 27 60 69.
veronique.bernard@inserm.fr

Running title: VAChT over-expression in striatal cholinergic interneuron

Keywords : ChAT–ChR2 mice, VAChT overexpression, cholinergic interneurons, cholinergic varicosities, electron microscopy, STED

Abbreviations :

ACh: Acetylcholine; AChE: Acetylcholinesterase; CathD: Cathepsin D; ChAT : Choline Acetyltransferase; CHC: Clathrin heavy chain; CHT: High-affinity choline transporter; ER: Endoplasmic Reticulum; CIN: Striatal cholinergic interneurons; GM130: Golgi matrix protein of 130kDa; IP : immunoparticle; PBS: Phosphate buffer saline; *pc*: Pearson's coefficient; PDI: protein disulphide isomerase; TGN38: Trans-Golgi network specific integral membrane protein; VAChT: vesicular acetylcholine transporter.

Title : Vesicular Acetylcholine Transporter (VAChT) overexpression induces major modifications of striatal cholinergic interneuron morphology and function

Abstract

Striatal cholinergic interneurons (CIN) are pivotal for the regulation of the striatal network. Acetylcholine (ACh) released by CIN is centrally involved in reward behavior as well as locomotor or cognitive functions. Recently, BAC transgenic mice expressing channelrhodopsin-2 (ChR2) protein under the control of the choline acetyltransferase (ChAT) promoter (ChAT–ChR2) and displaying almost 50 extra copies of the VAChT gene were used to dissect cholinergic circuit connectivity and function using optogenetic approaches. These mice display overexpression of the vesicular acetylcholine transporter (VAChT) and increased cholinergic tone. Consequently, ChAT–ChR2 mice are a valuable model to investigate hypercholinergic phenotypes. Previous experiments established that ChAT–ChR2 mice display an increased sensitivity to amphetamine induced-locomotor activity and stereotypies. In the present report, we analyzed the impact of VAChT overexpression in the striatum of ChAT-ChR2 mice. ChAT-ChR2 mice displayed increased locomotor sensitization in response to low dose of cocaine. In addition, we observed a dramatic remodeling of the morphology of CIN in ChAT-ChR2 transgenic mice. VAChT immunolabeling was markedly enhanced in the soma and terminal of CIN from ChAT-ChR2 mice as previously shown (Crittenden *et al.* 2014). Interestingly, the number of cholinergic varicosities was markedly reduced (-87%) whereas their size was significantly increased (+177%). Moreover, VAChT overexpression dramatically modified its trafficking along the somatodendritic and axonal arbor. These findings demonstrate that ChAT–ChR2 mice present major alterations of CIN neuronal morphology and increased behavioral sensitization to cocaine, supporting the notion that the increased levels of VAChT observed in these mice make them fundamentally different from wild-type mice.

Introduction

Acetylcholine (ACh) is a major neuromodulator of the striatal network. Dysfunctions of striatal cholinergic activity contribute to the pathophysiology of neurodegenerative diseases like Parkinson's disease or to the development of repetitive and compulsive behaviors, as well as to addiction (Di Chiara *et al.* 1994, Sakae *et al.* 2015, Zhao & Keen 2008, Ztaou *et al.* 2016). Although CIN represent less than 2% of striatal neurons, they display dense axonal arbors and release locally high levels of ACh (Lim *et al.* 2014). In CIN, ACh is transported into synaptic vesicles by the vesicular acetylcholine transporter (VAChT, *Slc18a3*). Therefore, VAChT is a pivotal actor of ACh-mediated neurotransmission (Prado *et al.* 2013). CIN also express the atypical vesicular glutamate transporter 3 (VGLUT3) and are able to release glutamate in addition to ACh (Gras *et al.* 2008, Sakae et al. 2015). Optogenetics has contributed to our improved understanding of specific neurochemical networks (Deisseroth 2015, Kreitzer & Berke 2011). It is still common for the study of cholinergic circuits the use of mouse lines expressing ChR2 under the ChAT promoter (Ren *et al.* 2011, Steidl *et al.* 2016, Wang *et al.* 2014, Zhao *et al.* 2011, Zhao & Keen 2008).

The cholinergic gene *locus* includes, between the first and second exons of the ChAT gene, an intronless open reading frame for VAChT (Cervini *et al.* 1995, Eiden 1998, Erickson *et al.* 1994, Roghani *et al.* 1994). Therefore, the BAC used to generate many reporter mouse lines (GFP, CRE and ChR2) carries also a copy of the VAChT gene (Crittenden et al. 2014, Kolisnyk *et al.* 2013, Ting & Feng 2014). Therefore, the ChAT-BAC mouse and rat lines overexpress VAChT in the striatum and other brain regions (Nagy and Aubert. 2013, Kolisnyk et al. 2013, Crittenden et al. 2014). Consequently, in these transgenic animals, ACh levels are increased in synaptic vesicles and there is significant increase in ACh release in the hippocampus and in their neuromuscular junction (Kolisnyk et al. 2013, Sugita *et al.* 2016). ChAT-ChR2 mice display marked improvement in motor endurance and cognitive deficits, including attention deficits and deficits in working and spatial memory (Kolisnyk et al. 2013). These mice also display an increase of amphetamine-induced stereotypies (Crittenden et al. 2014). Taken together, these results show that increased VAChT expression disrupts critical steps in information processing and exacerbates drug-induced behaviors.

Changes in cholinergic activity have the potential to cause long-term changes in neuronal function by disturbing gene expression pathways and critical signalling (Kolisnyk *et al.* 2013). For example, ChAT–ChR2 mice have increased levels of hnRNPA2/B1, an essential splicing regulator (Kolisnyk et al. 2016). However, although these abnormalities in gene expression in targeted tissues and behavioral functions are now documented, whether VAChT overexpression can have long-term consequences for cholinergic neuron function is

unknown. Elevated levels of VAChT could affect its own intraneuronal trafficking as well as that of other proteins.

Vesicular transporters undergo complex regulation of their trafficking, which has been well studied in the case of VAChT and vesicular monoamine transporters (VMAT1-2) (Barbosa *et al.* 2002, Fei *et al.* 2008, Ferreira *et al.* 2005, Krantz *et al.* 2000, Pothos *et al.* 2000, Santos *et al.* 2001, Santos *et al.* 2009, Tan *et al.* 1998, Yao & Hersh 2007). For example, VAChT follows the clathrin dependent endocytotic pathways before its targeting to varicosities (Tan *et al.* 1998, Krantz *et al.* 2000, Pothos *et al.* 2000, Santos *et al.* 2001, Barbosa *et al.* 2002, Ferreira *et al.* 2005, Fei *et al.* 2008, Santos *et al.* 2009).

In support to previous findings with amphetamine (Crittenden et al. 2014), we found that ChAT-ChR2 mice display increased behavioral sensitization in response to low dose of cocaine administration. Furthermore, VAChT overexpression dramatically remodelled CIN morphology and reduced the number and increased the size of cholinergic varicosities. Finally, we show that these mice presented altered VAChT trafficking in CIN. Our findings show functional changes and long-term modification of CIN morphology presumably due to VAChT overexpression. Furthermore, our results stress the need for careful use of ChAT-ChR2 mice and other ChAT-BAC transgenic rodents for functional and imaging experiments.

Methods

Animals

Experiments followed the Canadian Council of Animal Care (CCAC) guidelines for care and use of animals. The animal protocol was approved by the University of Western Ontario (protocol # 2008-127). ChAT-ChR2 mice [B6.Cg-Tg(Chat-COP4*H134R/EYFP)6Gfng/J; The Jackson Laboratory] were described previously (Ting & Feng 2014, Zhao *et al.* 2011). Mice were maintained as hemizygous on C57BL/6J background. Only male mice were used in the study and wildtype (WT) littermates were used as controls.

For behavioral experiments, animals were housed in groups of two to four per cage in a temperature-controlled room (22-23°C) with a 12:12 light–dark cycle (lights ON at 7am). Food and water were provided ad libitum. Mice older than 2 months were used in all experiments and the age range in individual behavioral experiments was as follows: behavioral sensitization experiments without habituation 2-3 months; behavioral sensitization experiments in which mice were habituated to locomotor boxes 2-5 months (cocaine 10 mg/kg) and 3-7 months of age (cocaine 20 mg/kg). Mice were randomized into treatment groups using a randomization table and the experimenter was blind to the genotypes [ARRIVE guidelines (Kilkenny *et al.* 2010)].

Behavioral experiments

Determination of sample size in behavioral experiments

The initial data from the first behavioral sensitization experiment (protocol without habituation, see below) were used to determine the expected difference between genotypes (approximately 20%) and the approximate standard deviation associated with the measurements. Based on these values we calculated the number of animals required for the statistical power of 0.8 as minimum of 10 mice per each group. The sample size and statistical power was calculated for repeated measures ANOVA test that was later used for statistical analysis. We used G*Power software (Faul *et al.* 2009) to calculate sample sizes and statistical power.

Behavioral sensitization

Two complementary protocols with or without habituation to the locomotor boxes were used to assess behavioral sensitization to cocaine. In experiments in which mice were not habituated, the animals were repeatedly injected intraperitoneally with cocaine (i.p., 10 mg/kg in 0.01 ml/g) in six successive days (day 1-6). After each injection, mice were immediately placed into the open field apparatus and locomotor activity was measured for 1 hour. An automated activity monitor (AccuScan Instruments Inc.; Columbus, OH; 20 cm x 20 cm

platform with 30 cm high walls) was used to measure locomotor activity. Distance travelled (converted from beam breaks to cm) was recorded at 5-min blocks and the first 20 minutes after injection were used for analysis (Guzman *et al.* 2011).

In our second experimental design, mice were first habituated to the open field apparatus and to i.p. injection by receiving saline injection repeatedly for 3 successive days (day 1-3). Mice were habituated to the apparatus 60 minutes before the injection then removed from the apparatus for injection and immediately placed back after injection. Locomotion was recorded 60 minutes before and after injection but only the first 30 minutes after injection were used for analysis. From day 4, mice were separated into 2 groups: group 1 (saline) continued to receive saline injections while group 2 (cocaine) received cocaine i.p. injections (10 or 20 mg/kg in 0.005 ml/g) in five successive days (day 4-8). After the injection on day 8, mice were left undisturbed in their cages for the subsequent 4 days. All mice (group 1 and 2) received a last cocaine injection on day 13. Locomotion was recorded and analysed as described above in the same apparatus.

In all 3 experiments together, one mouse was excluded because it died during experiment and two were excluded (from experiment 1 and 2, cocaine treated and one saline treated respectively) as outliers, based on the formula: group average $\pm$ 2x standard deviation.

Tissue preparation for immunohistochemistry

For all anatomical studies we used 2-5 months old male mice. Stimulated-emission-depletion (STED) and electron microscopy (EM) experiments were performed on WT and ChAT-ChR2 mice. Briefly, animals were deeply anesthetised and perfused transcardially with paraformaldehyde (2%). For EM experiments, 0.2% glutaraldehyde was added in the perfusion solution. Brains were dissected, fixed over-night in 2% paraformaldehyde and stored in PBS until use. Sections (70 μm-thick) from forebrain including striatum were cut on a vibrating microtome (Leica, VT1000S).

Antisera

VAChT was detected with an anti-VAChT polyclonal antiserum raised in guinea pig (Gras et al. 2008). VGLUT3 was detected with an anti-VGLUT3 polyclonal antiserum raised in rabbit (Synaptic Systems Cat# 135 203 Lot# RRID:AB_887886). To identify subcellular compartments associated with VAChT, the following antisera were used: anti-Clathrin heavy chain (CHC ; mouse ; BD Biosciences Cat# 610499 Lot# RRID:AB_397865) ; anti- trans-Golgi network specific integral membrane protein (TGN38, mouse; Thermo Fisher Scientific Cat# MA3-063 Lot# RRID:AB_325484); anti-Golgi matrix protein of 130kDa (GM130; mouse; BD Biosciences Cat# 610822 Lot# RRID:AB_398141); anti-Rab5 (mouse; BD Biosciences Cat# 610281 Lot# RRID:AB_397676); anti-Rab9 (mouse; Thermo Fisher Scientific Cat#

MA3-067 Lot# RRID:AB_2175599); anti-protein disulphide isomerase (PDI; mouse; Thermo Fisher Scientific Cat# MA3-019 Lot# RRID:AB_2163120); anti-cathepsin D (CathD (G-19); mouse; Santa Cruz Biotechnology Cat# sc-6494 Lot# RRID:AB_2087097). The following markers of the cholinergic system were used: anti-choline acetyltransferase (ChAT; goat; Millipore Cat# AB144P Lot# RRID:AB_2079751), anti-acetylcholinesterase (AChE, a gift from Palmer Taylor, UCSanDiego, USA), anti-high-affinity choline transporter (CHT; mouse; Synaptic Systems Cat# 216 011 Lot# RRID:AB_2301977).

The specificity of VAChT labelling was assessed by the disappearance of the staining in VAChT null mice (data not shown, Guzman et al. 2011).

Immunofluorescent detection of VAChT at confocal microscopic level

VAChT was detected alone or in association with VGLUT3 or with various markers of subcellular compartments in perikarya and axonal varicosities of CIN of the mouse striatum. Sections were incubated with antisera against: VAChT (1:5000) and VGLUT3 (1:1000), CHC (1:500), TGN38 (1:500), GM130 (1:200), Rab5 (1:100), Rab9 (1:500), PDI (1:100), AChE (1:1000), CHT (1:300), CathD (1:1000), ChAT (1:300). Sections were then incubated in a mixture of secondary antibodies: goat anti-guinea pig coupled to Alexa 594 for VAChT detection (1:1000, Molecular Probes Cat# A-11076 also A11076 Lot# RRID:AB_141930) and goat anti-mouse (for CHC, TGN38, GM130, Rab5, Rab9, PDI, CHT; 1:1000, Thermo Fisher Scientific Cat# A10524 Lot# RRID:AB_2534033) or goat anti-rabbit (for AChE and VGLUT3; 1:1000, Thermo Fisher Scientific Cat# A10523 Lot# RRID:AB_2534032); all coupled to CY5. For the simultaneous detection of VAChT and ChAT or CathD, sections were first incubated with a donkey anti-goat coupled to Alexa 633 (ChAT or CathD; 1:1000, Molecular Probes Cat# A-21082 also A21082 Lot# RRID:AB_141493), washed 3 times in PBS, incubated in 4% normal goat serum, then in goat anti-guinea pig coupled to Alexa594 (VAChT), washed in PBS, and mounted in Prolong gold (ThermoFisher Scientific). Sections were observed using an inverted TCS SP5 confocal microscope (Leica Microsystems) equipped with a 63X HCX Plan APO CS NA=1.4 oil immersion objective. The pixel size was set to 60 nm and two diode lasers at 561nm and 633nm were used. VAChT labeling was first identified by epifluorescence under the confocal microscope using a filter specific for the red fluorochrome (filter N2.1, Bandpas 515-560 nm dicroic: 580, Longpass 590 nm). Images were acquired in the confocal mode. The confocal microscope used an Acousto-Optical Beam Splitter (AOBS) system without any filter of excitation. Two laser diodes were used: DPSS: 561 nm, 10mW and HeNe : 633 nm, 10mW to excite Alexa594 and 633 fluorochromes, respectively.

The cross-talk and bleed through between channels were minimized by two means.

First, we have chosen the spectra band of emission of Alexa594 in order to avoid to collect emission due to the excitation of Alexa633 or CY5 by the 561nm laser. The spectra band to

detect emission of Alexa594 was set to 570-615nm for Alexa594-Alexa633 colocalization experiments. The spectra band to detect emission of Alexa594 was set to 570-620nm for Alexa594-CY5 colocalization experiments. The spectra band to detect emission of Alexa633 and CY5 was set to 660-711nm.

Second, we have checked that no signal was detected in the Alexa633/CY5 or Alexa594 channels when Alexa594 or Alexa633/CY5 were excited in single labeled sections.

Images were treated using ImageJ and Adobe Photoshop software.

Immunofluorescent detection of VAChT at STED microscopic level

Sections were successively incubated in anti-VAChT guinea pig polyclonal antiserum (1:5000) overnight then with goat anti-guinea pig IgG coupled to Alexa 594 (1:100; ThermoFisher Scientific) and mounted in ProLong Gold (Thermo Fisher Scientific).

Sections were observed using a SP8 gated-STED 315 microscope (Leica Microsystems) equipped with a 775nm depletion laser. Alexa 594 was excited at 594nm. All acquisitions were performed using the same excitation laser power (2%). Sequential scanning of individual channels has been used in all colocalizations analyses. Images were submitted to deconvolution (Huygens software, Scientific Volume Imaging) that allows the recovery of objects that are degraded by blurring and noise. Finally, images were analyzed using ImageJ (National Institutes of Health) and Adobe Photoshop.

Quantification of the density, surface and intensity of VAChT immunopositive-spots

Striatal sections labeled for VAChT immunoreactivity were observed using the 63x objective and acquisitions were performed under the confocal microscope using the same excitation laser intensity and parameters for WT and ChAT-ChR2 mice sections. Labeling was then analyzed using the ImageJ software (National Institutes of Health). Because of the VAChT overstaining in ChAT-ChR2 mice, overlapping immunopositive puncta could not be resolved leading to lower quantal counts. To correct this bias, we analyzed our images using a method that allows separation of touching fluorescent objects. This method, called the watershed separation, is performed with the ImageJ software. Briefly, after thresholding, the objects (here varicosities) are separated from the background (Fig. S1b, g). Then, varicosities are separated one from another, with the watershed function (Fig. S1d,i) and counted with the analyze particles function (Fig. S1e,j). The density of VAChT immunopositive spots and of the surface of cholinergic varicosities were quantified. For that, seventy five fields (surface: 655µm^2) in striatum per animal in 6 mice per group were acquired under the confocal microscope.

The relative optical density corresponding to the relative intensity of spots was automatically calculated by the ImageJ software.

Quantification of Colocalization.

In perikarya, the quantification of colocalization of VAChT with organelle or cholinergic markers was analyzed with the "Just Another Colocalization Program" (JACoP) plug-in (ImageJ, National Institutes of Health), and statistical data are reported from the Costes's randomization-based colocalization module (Bolte & Cordelieres 2006). Costes's randomization method for measurement of colocalization was used to confirm, with >95% certainty, that the colocalization observed between the VAChT and organelle or cholinergic markers immunofluorescent signal was not caused by chance coincidence (Costes *et al.* 2004). A Pearson's coefficient (*pc*) was calculated. Costes' randomization was applied on 5 neurons from 4 mice of each genotype using at least 150 iterations per image. Analysis have been restricted to the somatic area. Just individual images were analyzed.

In varicosities, the quantification of colocalization of VAChT with organelle markers was performed from the labeling on image observed with the 63x objective (surface of the field: 655µm^2). Labeling was then analyzed using the ImageJ software (National Institutes of Health). Briefly, after thresholding, puncta labeling (i.e. varicosities) were automatically cropped and touching varicosities were separated by the watershed function (see above). Their number was automatically calculated. Every image was carefully analyzed and the number of puncta displaying labeling for both VAChT and another protein was marked using the cell counter pluggin of ImageJ (National Institutes of Health). Results were expressed as the percentage of VAChT immunoreactive spots, displaying also labeling for a marker of organelles. Three images (surface of the field: 655µm^2) from 4 mice of each genotype were quantified. A mean of 2018 varicosities per WT mouse and 558 varicosities ChAT-ChR2 animal were analyzed.

Electron microscopy

Electron microscopic experiments were performed on WT and ChAT-ChR2 mice brain tissue as previously described (Bernard *et al.* 1998). Briefly, animals were deeply anesthetized and perfused transcardially with a mixture of 2% paraformaldehyde in 0.1 M phosphate buffer (pH7.4) and 0.2% glutaraldehyde. Brains were dissected, fixed overnight in 2% paraformaldehyde and stored in PBS until use. Sections (50 *µ*m) from midbrain including striatum were cut on a vibrating microtome (Leica, VT1000S). Sections were successively incubated in anti-VAChT guinea pig polyclonal antiserum (1:5000), then with goat anti-guinea pig IgG coupled to biotin (Vector laboratories) and in streptavidin coupled to gold particles (1.4 nm in diameter; Nanoprobes; 1:100 in a buffer containing PBS, bovine serum albumin and gelatin). The signal of the gold immunoparticles was increased using a silver enhancement kit (HQ silver; Nanoprobes) for 2 min at RT in the dark. Finally, after treatment

of sections with 1% osmium, dehydration and embedding in resin, ultrathin sections were cut, stained with lead citrate and examined with a transmission electron microscope (EM 912 OMEGA, Zeiss) equipped with a LaB6 filament at 80kV. Images were captured with digital camera (SS-CCD, 2kx2k, Veleta). Alternatively, a Field Emission scanning electron microscope GeminiSEM 500 (Zeiss) operating at 20kV with a 20µm aperture was also used. Transmitted electrons are collected in bright field mode with the STEM detector located beneath the sample. Finally, the surface of axonal varicosities labeled for VAChT and the surface of their mitochondria were measured using ImageJ.

Quantification of the surface of varicosities and mitochondria and of VAChT-immunoparticles for VAChT at EM level

The quantification of the surface of varicosities and mitochondria was performed from EM images with the ImageJ software. As an index of the relative number of VAChT molecules per varicosity at EM level, we have quantified the surface occupied by immunoparticles (IPs) per surface of varicosity. The number of IPs is proportional to the quantity of molecules detected (as previously validated (Bernard *et al.* 2003, Bernard *et al.* 1999)). Briefly, after thresholding at the same level for both genotypes of labeled varicosities on EM images, black dots corresponding to IP were automatically cropped and their surface was calculated. These values were divided by the surface of varicosities (excluding the surface occupied by mitochondria).

Statistical analyses

Statistical analysis of behavioral experiments was done with Prism 7 software (Graph Pad). Student's *t* test was used to compare total distance travelled after the first cocaine injection. Two-way analysis of variance (ANOVA) was used to evaluate the effect of cocaine dose (10 or 20mg/kg) on the total distance travelled on day 8 of behavioral sensitization in the control and mutant mice. Repeated measures two-way ANOVA was used to evaluate the effect of genotype on the distance travelled throughout the behavioral sensitization experiments. Bonferroni's test was used for post hoc comparisons. P values < 0.05 were considered as statistically significant.

Statistical analyses for anatomical investigations were performed with Prism 4 software compare (Graph Pad). The density of VAChT immunoreactive spots, the surface of varicosities and mitochondria, the surface of IP for VAChT and the *pc* calculated in colocalizations analyses in WT and ChAT-ChR2 were compared using a Mann-Whitney U test. The percentage of VAChT immunopositive varicosities expressing markers of organelles were compared using the Fisher's exact test. All data are shown as the means ± SEM; * $p < 0.01$; **: $p<0.005$; ***: $p<0.0001$.

Results

ChAT-ChR2 mice are more sensitive to cocaine

ChAT-ChR2 mice have more pronounced repetitive behavior after administration of amphetamine (Crittenden et al. 2014). To test whether ChAT-ChR2 mice have abnormal responses to other psychostimulants, ChAT-ChR2 mice and WT littermates (n=8 for each genotype) were injected with cocaine (i.p., 10 mg/kg) daily during 6 successive days. Locomotor sensitization was measured (Fig. 1a). On the day 1, we saw no significant difference in locomotor activity between groups (mean±SEM of total distance traveled in 20 minutes after first injection for controls and mutants, respectively: 571±132 and 756±133 cm; $t_{(14)=}$0.989, p=0.34, two-tailed t test) (Fig. 1a). However, after repeated administrations of cocaine on days 2-6, ChAT-ChR2 mice showed increased activity compared to wildtype littermates (repeated measures ANOVA main effect of genotype F(1, 14)=18.07; p=0.0008) (Fig. 1a). Moreover, post-hoc analysis with Bonferroni's multiple comparisons test showed that the ChAT-ChR2 mice moved significantly more than controls already on the day 2 (mean±SEM of total distance traveled for controls and mutants, respectively: 1109±169 and 2185±222, p=0.0052).

To further test abnormal behavioral sensitization in ChAT-ChR2 mice, we used a new cohort of mice. We first habituated them extensively to locomotor boxes, handling and injections. This protocol was used to separate the specific effect of drug on behaviour sensitization from the effect of novelty. As can be seen, WT mice and ChAT-ChR2 mice receiving only saline injection showed no locomotor sensitisation (Fig. 1b). In contrast, ChAT-ChR2 mice presented increased behavioural sensitization after cocaine injection (repeated measures ANOVA main effect of genotype, $F_{(1,\ 20)}$=7.875; p=0.0109) (Fig. 1b). The *post-hoc* analysis (Bonferroni's multiple comparisons test) revealed that the ChAT-ChR2 mice receiving cocaine were significantly different from wildtype mice receiving cocaine after the third injection of cocaine on day 6 (mean±SEM of total distance traveled for controls and mutants, respectively: 576±157 and 1416±255, p=0.0378). There also appeared to be a trend towards hyperactivity in ChAT-ChR2 mice during the habituation period and after the first injection of cocaine that was not statistically significant (difference in locomotion between genotypes on day 4 $t_{(180)}$=1.896, adjusted p=0.536, Bonferroni's *post-hoc* test).

We also tested whether the increased behavioral sensitization of ChAT-ChR2 mice is dose-dependent or if the mice show increased sensitization to both low and high doses of cocaine. For this, a new cohort of WT mice and ChAT-ChR2 mice were injected with 20 mg/kg (i.p.) of cocaine. As expected, the sensitization elicited in both WT and ChAT-ChR2 mice by 20 mg/kg of cocaine was higher than the sensitization elicited by 10 mg/kg (mean±SEM of

distance travelled on the day 8 after 10 mg/kg in wildtypes and mutants, respectively: 762±202 and 1719±307; and after 20 mg/kg in wildtypes and mutants, respectively: 4205±471 and 3858±465; two-way ANOVA main effect of cocaine dose, $F(1, 39)=54.3$, $p<0.0001$). However, the locomotion of ChAT-ChR2 and control mice after cocaine administration was almost identical throughout the experiment (Fig. 1c). High doses of stimulants such as the one used here can also induce stereotypies in mice which would result in decreased locomotion. Because we did not visually evaluate stereotypies in our experiment we cannot exclude the possibility that while the locomotion appeared to be the same, the ChAT-ChR2 mice were actually displaying more stereotypies and thus higher sensitivity to cocaine. Therefore, based on our data, we can only conclude that ChAT-ChR2 mice are more sensitive to low doses of cocaine.

VAChT expression is dramatically modified in striatum of ChAT-ChR2 mice.

Given the predominant role of the striatum in the response to drugs of abuse, we investigated the expression of VAChT and morphology of CIN. Using confocal microscope, VAChT is observed in the soma of scattered large-sized neurons in the striatum of WT mice (Fig. 2a, a'). In addition, VAChT-immunolabelling is also present abundantly as punctiform labeling corresponding to staining in axonal varicosities (Fig. 2a, a'; arrows). A similar distribution is observed in the dorsal striatum as well as in the nucleus accumbens (data not shown). As shown in Fig. 2b, b', VAChT labelling is dramatically modified in ChAT-ChR2 mice. The intensity of VAChT immunolabeling is strongly increased in both soma and varicosities, as expected, due to overexpression. In perikarya of ChAT-ChR2 mice, VAChT staining was detected in large puncta in the cytoplasm and close to the plasma membrane. Furthermore, the number of VAChT-immunopositive varicosities seemed dramatically reduced compared to WT animals (Fig. 2b; -87 %; WT: 0.957±0.038 immunoreactive spots/μm^2; ChATChR2 : 0.125±0.016 immunoreactive spots/μm^2; Mann–Whitney U test: $p<0.01$; n=6 mice per group). It is possible that individual puncta visible in the control mice are overlapping in the BAC mice, leading to lower quantal counts only because they cannot be resolved. We have used an additional marker, VGLUT3 staining, to confirm that the decrease of our quantification concerning VAChT varicosities is real. Indeed VGLUT3 and VAChT are co-expressed in CIN varicosities (see Gras et al. 2002 for example). Interestingly, in contrast to VAChT, VGLUT3 immunolabeling intensity is unchanged in CIN from ChAT-ChR2 mice relatively to WT mice (Fig. 2 c-d'; Relative optical density in varicosities: WT: 26.16±1.14; ChATChR2 : 26.43±1.59; Mann-Whitney U test : NS, n=6 for each genotype). Importantly, the decreases of the density of VAChT and VGLUT3 varicosities in ChAT-ChR2 mice are similar (-87% and -74%, respectively). These data

support the notion that the number of cholinergic varicosities is reduced in mice over-expressing VAChT, likely impacting both VAChT and VGLUT3 neurotransmission.

In addition, the surface of cholinergic VAChT immunopositive varicosities is significantly higher in mutant mice compared to WT animals (Fig. 2b; +177%; WT: 0.060±0.006µm^2; ChATChR2 : 0.165±0.010 µm^2; Mann–Whitney U test: p<0.01).

In order to increase the resolution and better resolve how additional VAChT-positive material is distributed in cholinergic axonal varicosities of ChAT-ChR2 mice, we used super-resolution STED microscopy (Fig. 2e-l). At low magnification, we detected small spots of VAChT immunolabeling in varicosities of WT mice (Fig. 2e). In contrast, in ChAT-ChR2 mice, varicosities are much larger and VAChT labeling is observed at the periphery of the varicosities (Fig. 2f, arrows). At higher magnification, STED experiments show groups of labeled spots in varicosities in WT mice, (Fig. 2g,h,i). In contrast, in the enlarged boutons from CIN of ChAT-ChR2 mice, immuno-positive spots seemed clustered at the periphery (Fig. 2j,k,l). This was confirmed by EM experiments (Fig. 3h,i).

In summary, our data show that ChAT-ChR2 mice have a lower number of larger cholinergic striatal varicosities when compared to controls and that VAChT is located mostly at the periphery of these large boutons in ChAT-ChR2.

Ultrastructural localization of VAChT in ChAT-ChR2 mice

We performed pre-embedding immunogold detection, in order to determine with a higher resolution VAChT localization and its distribution within CIN. EM observations demonstrated that in WT mice, VAChT is exclusively associated with membranous organelles in the perikarya and varicosities (Fig. 3 a, c, e and f). In perikarya, some IPs for VAChT are associated with the endoplasmic reticulum (ER) and Golgi apparatus (Go) (Fig. 3a arrows, c). In ChAT-ChR2 mice, a higher density of IP is identified in perikarya in association with ER and Go (Fig. 3b (arrows), d). VAChT is also detected at the surface of large-sized vesicles in the perikarya (Fig. 3, b', b''). EM observations confirmed the substantial increased size of axonal varicosities in mutant mice (Fig. 3j; +177%, Mann–Whitney U test: p<0.01; n=6 mice in each group). In WT mice, VAChT IP are evenly distributed inside the axonal varicosities and are associated with synaptic vesicles (Fig. 3 e, f; arrow-heads). In ChAT-ChR2 mice, the density of VAChT IP was dramatically increased and often located underneath the plasma membrane (Fig. 3h,i). Because of the size of the IP (20nm in diameter), it was difficult to determine whether VAChT is associated with plasma membrane, or with sub-membranous organelles that may be hidden by the high density of IP. Within enlarged cholinergic varicosities, the clustering of VAChT IP prevented quantitative analysis of synaptic vesicles (Fig. 3h,i). We found a significant increase of the surface occupied by IP in cholinergic varicosities of ChAT-ChR2 mice compared to WT mice (+108%, WT: 0.1128±0.0185; ChAT-

ChR2: 0.2344±0.0164; n=6, Mann-Whitney U test p<0.01), suggesting an increase of VAChT molecules in mutants.

Of the 41 varicosities observed in ChAT-ChR2 mice, 17 (41%) of them contained one large round-shaped compartment (Fig. 3g). Of 10 perikarya observed, all of them contained a mean of 12 large round-shaped compartments (Fig. 3b,b',b').

Surprisingly, the number of mitochondria per varicosity appeared increased in ChAT-ChR2 mice relatively to WT mice. Indeed, only 16% out of 120 VAChT immunopositive varicosities in WT mice contain one mitochondrion. In contrast, 65% of 125 varicosities in ChAT-ChR2 mice contain at least one mitochondrion and some of them showed two mitochondria. Moreover, the quantification demonstrated that the surface of mitochondria in ChAT-ChR2 mice is increased compared to WT animals (Fig. 3k; +93%; Mann–Whitney U test: p<0.01). In summary, the overexpression of VAChT in ChAT-ChR2 mice profoundly alters the shape and organization of cholinergic striatal varicosities.

VAChT overexpression induces redistribution of VAChT in subcellular compartments

The trafficking of VAChT has been previously investigated (Santos et al. 2001; Barbosa et al. 2002, Kim & Hersh 2004, Ferreira et al. 2005). We then investigated whether over-expression of VAChT would impact its synthesis in the ER, maturation in Golgi apparatus, endocytosis in clathrin coated pits in perikarya and varicosities of ChAT-ChR2 mice.

Colocalization of VAChT and organelle or cholinergic markers in perikarya were analyzed (Bolte & Cordelieres 2006, Costes et al. 2004) (see methods). Colocalization observed between the VAChT and organelle or cholinergic markers immunofluorescent signal was not caused by chance coincidence in all WT and ChAT-ChR2 and for all combination of markers. In WT mice, PDI, GM130 or TGN38, specific markers of the endoplasmic reticulum, cis- or trans-Golgi apparatus, respectively, were detected in small proportion in subcellular compartments expressing VAChT (Fig. 4a,c,e,g,i,k; Fig. S2; Fig. S3; *pc* = 0.32±0.01, 0.34±0.04 or 0.24±0.03, respectively). The colocalization of VAChT with PDI, GM130 and TGN38 (Fig. 4b,c,f,g,j,k, arrow-heads; *pc* = 0.66±0.05, 0.53±0.01 or 0.70±0.05, respectively) was significantly higher in perikarya of ChAT-ChR2 mice compared to WT mice (Mann–Whitney U test: $p < 0.0001$). In varicosities of WT mice, PDI, GM130 or TGN38 were detected in a very weak proportion of VAChT immunopositives varicosities (Fig. 4a',d,e',h,i' and l; 3.45%±1.45, 0.26%±0.08 or 1.30%±0.42, respectively). In contrast, in ChAT-ChR2 mice, PDI, GM130 or TGN38 were present in almost all VAChT immunopositives varicosities (Fig. 4b',d,f',h,j' and l; 94.91%±1.17, 98.48%±0.52 or 95.78%±0.35, respectively). The Fisher's test demonstrated a highly significant increase in the proportion of varicosities expressing VAChT and PDI, GM130 and TGN38 (Fig. 4d,h,l; $p < 0.0001$).

In soma or varicosities of WT animals, clathrin heavy chain (CHC), Rab5 or Rab9, markers of clathrin-coated pits or early or late endosomes, respectively, were rarely detected in VAChT immunopositive puncta (Fig. 5a,a',e,e',i and i'; perikarya : *pc* = 0.27±0.03, 0.26±0.01 and 0.29±0.03, respectively; varicosities : 2.96%±0.47, 3.67%±0.11 or 2.49%±0.30, respectively). In contrast, in perikarya and varicosities from the striatum of ChAT-ChR2 mice, CHC, Rab5 and Rab9 were often detected in subcellular compartments immunopositive for VAChT (Fig. 5b,b',c,d,f,f',g,h,j,j',o and p; Fig. S3; Fig. S5; arrow-heads; perikaya: *pc*= 0.56±0.08, 0.67±0.03 and 0.71±0.05, respectively; varicosities : 94.52%±1.75, 94.22%±1.97 and 94.47%±1.03, respectively). The colocalization of VAChT with CHC, Rab5 and Rab9 was significantly higher in perikarya of ChAT-ChR2 mice compared to WT mice (Fig. 5c,g and k; Mann–Whitney U test: $p < 0.0001$). The Fisher's test demonstrated a highly significant increase in the proportion of varicosities expressing VAChT and CHC, Rab5 and Rab9 (Fig. 5d,h,l; $p < 0.0001$).

Finally, in WT mice, CathD, a marker of lysosomal vesicles, was detected in VAChT expressing compartments in the soma or varicosities of CIN (Fig. 5m,m' and o; perikarya : *pc*= 0.46±0.04; varicosities : 0.47%±0.14), whereas this was occasionally the case in the striatum of ChAT-CHR2 mice (Fig. 5n and n'). In perikarya and varicosities from the striatum of ChAT-ChR2 mice, CathD was often detected in subcellular compartments immunopositive for VAChT (Fig. 5n,n',o, and p; arrow-heads; perikaya: *pc*= 0.76±0.02; varicosities : 98.54%±0.60). The colocalization of VAChT with CathD is significantly higher in perikarya of ChAT-ChR2 mice compared to those from WT (Fig. 5o; Mann–Whitney U test: $p < 0.0001$). The Fisher's test demonstrated a significant increase in the proportion of varicosities expressing VAChT and CathD (Fig. 5p; $p < 0.0001$). These data demonstrate that in ChAT-ChR2 mice, overexpressed VAChT is largely redistributed in CIN and overflows to the endoplasmic reticulum, cis- and trans-Golgi apparatus, clathrin-coated pits, in early and late endosomes and lysosomes.

VAChT overexpression does not modify expression of cholinergic markers

We next inspected whether VAChT overexpression impacted the expression of other cholinergic markers, such as ChAT, AChE and CHT in CINs of ChAT-ChR2 mice.

The intensity of the immunolabeling of ChAT, AChE, and CHT were quantified in WT and in ChAT-ChR2 mice at the level of varicosities and perikarya. We observed no modification of the intensity of the various immunolabeling (Relative optical density in varicosities: ChAT : WT: 16.73±0.63; ChATChR2 : 14.84±0.27; AChE : WT: 27.71±2.16; ChATChR2 : 27.45±2.045; CHT : WT: 32.20±3.07; ChATChR2 : 31.99±2.79; For all three markers : Mann-Whitney U test : NS, n=4 for each genotype).

In perikarya of WT mice ChAT immunoreactivity was homogeneously detected in the cytoplasm of cell bodies (Fig. 6a). Labeling was detected in the cytoplasm which sometimes colocalized with VAChT (Fig. 6a,c; *pc*=0.49±0.06). AChE immunoreactivity was detected mostly at the plasma membrane of perikarya (as previously shown, (Dobbertin *et al.* 2009) (Fig. 6d; arrows). A faint staining was detected in the cytoplasm that sometimes colocalized with VAChT (*pc*=0.42±0.01). As previously established (Ferguson *et al.* 2003, Ribeiro *et al.* 2003), CHT immunoreactivity was detected mostly in the cytoplasm, in vesicles-like structures in perikarya (Fig. 6g), sometimes associated with VAChT staining (*pc*=0.60±0.04). The same pattern was generally observed in ChAT-ChR2 mice, however, ChAT, AChE and CHT showed partial colocalization with VAChT (Fig. 6b,c,e,f,h,i; arrow-heads; *pc*=0.80±0.05, 0.69±0.03 and 0.88±0.02). The colocalization of VAChT with ChAT, AChE and CHT is significantly increased in perikarya of ChAT-ChR2 mice compared to those from WT mice (Fig. 6c,f and i; Mann–Whitney U test: $p<0.0001$).

Discussion

The gene encoding for VAChT is embedded within the first intron of the ChAT gene (Cervini et al. 1995, Eiden 1998, Erickson et al. 1994, Roghani et al. 1994). The ChAT-ChR2 mouse line incorporated almost 50 extra copies of the VAChT gene (Kolisnyk et al. 2013). Hence, this mouse line is a convenient model to study the functional and anatomical consequences of hyper-cholinergy. This is particularly relevant in the striatum, the brain area with the highest content in ACh. The increase in VAChT expression augments ACh storage and release from synaptic vesicles in the neuromuscular junction and in the brain (Kolisnyk et al. 2013, Sugita et al. 2016). Interestingly, mutations in VAChT in humans (O'Grady et al., 2016; Aran et al., 2017) phenocopy mice with decreased levels of VAChT suggesting a high degree of functional conservation (Aran *et al.* 2017, Lima Rde *et al.* 2010, Martyn *et al.* 2012, O'Grady *et al.* 2016, Prado *et al.* 2006, Roy *et al.* 2013). We show in the present paper that overexpression of VAChT, consistently with changed cholinergic function, increases behavioral sensitization in response to cocaine administration. Moreover, ChAT-ChR2 BAC mice display profound alterations in cholinergic neuropil within the striatum, likely due to VAChT spilling over to several different membranous compartments involved with the synthesis and trafficking of membrane proteins.

VAChT overexpression induces increased behavioral sensitization in response to cocaine administration.

VAChT overexpression disrupts a number of cognitive functions, presumably due to excessive increase in cholinergic tone (Kolisnyk et al. 2013). In addition, ChAT-ChR2

response to amphetamine is also altered as the mice are more prone to amphetamine-induced stereotypies and show increased behavioral sensitization induced by low doses of amphetamine (Crittenden et al. 2014). The present study supports and further extends these observations, by showing that these mice also show increased behavioral sensitization induced by low doses of cocaine.

The mechanism by which the putative increased cholinergic tone affects the responses to stimulants is not fully understood, but it is likely to be mediated by increased VAChT levels in ChAT-ChR2 BAC mice. Although several brain regions contribute to behavioral sensitization to cocaine (e.g. medial prefrontal cortex, ventral tegmental area or pedunculopontine and laterodorsal tegmental nucleus, both containing cholinergic neurons), the nucleus accumbens (ventral striatum) is usually seen as a key structure controlling increased motor response to repeated administration of stimulant drugs (Steketee and Kalivas, 2011). However, the relationship between striatal ACh and sensitivity to cocaine is complex and cocaine-induced effects can be both decreased and increased as a result of cholinergic manipulations (Gonzales & Smith 2015, Williams & Adinoff 2008). It should not be surprising then that while ablation of striatal CINs leads to higher sensitivity to cocaine (Hikida *et al.* 2003, Kitabatake *et al.* 2003), the ChAT-ChR2 mice with putative increase in cholinergic tone display a similar effect. Some of the conflictual observations can probably be explained by the fact that CIN release glutamate in addition to ACh (El Mestikawy *et al.* 2011, Gras *et al.* 2002). Therefore, glutamate released by CINs could account for some effects previously attributed to ACh in CIN ablation experiments (Guzman et al. 2011, Sakae et al. 2015). Deleting VGLUT3, which alters the balance between glutamate and ACh, increases sensitivity to cocaine psychostimulant effects (Gras et al. 2002, Sakae et al. 2015). Increased VAChT expression may change the balance between ACh and glutamate released by CIN similar to removal of VGLUT3. Alternatively, increased VAChT expression may have long-term effects in gene expression as we previously observed (Kolisnyk et al. 2016). This may also contribute to the profound morphological changes we detected in these cholinergic interneurons as discussed below.

VAChT overexpression induces deep remodeling of striatal cholinergic interneurons morphology

VAChT overexpression deeply remodels the morphology of CIN. Changes induced by VAChT overexpression are particularly spectacular at the level of axonal varicosities as shown by the increased size of axonal varicosities. The molecular and cellular pathways underlying the enlargement of axonal varicosities is not yet determined. However, it can be hypothesized that these modifications could result from a putative cholinergic overactivity

induced by VAChT overexpression. Cholinergic overactivity was described in the hippocampus and neuromuscular junction of mice over-expressing VAChT (Kolisnyk et al. 2013, Sugita et al. 2016). However, this is not yet formally established in the striatum of ChAT-ChR2 mice.

Our morphological observations lead to a central question: can putative cholinergic overactivity be responsible for these changes of axonal morphology? Interestingly, another mutant mouse line, which lacks the proline-rich membrane anchor (PRIMA) for AChE has ≈ 90% loss of AChE activity (Dobbertin et al. 2009). Genetic ablation or pharmacological inhibition of AChE is a classic method to increase ACh transmission (Mount *et al.* 1994, Ray *et al.* 2009). Interestingly CIN varicosities were not altered in PRIMA-KO (Dobbertin et al. 2009). However, it should be noted there might be important differences between these mouse lines regarding cholinergic tone. PRIMA-KO mice have substantial receptor desensitization, likely due to constant increased levels of ACh in the synaptic cleft. ChAT-ChR2 mice in contrast release more ACh, but the neurotransmitter can be quickly degraded in synapses, as AChE activity and expression is not altered (present findings and (Sugita et al. 2016)). ChAT-ChR2 mice are unlikely to present similar levels of receptor dysfunction as PRIMA-KO, although we did detect substantial change in M2 autoreceptors that are consistent with downregulation or desensitization. Alternatively, it cannot be excluded that compensatory mechanisms prevent generalized cholinergic overactivity and that these effects are independent from cholinergic tone. Therefore, the formal confirmation (or information) of the existence of an overactive cholinergic tone will be necessary to fully interpret the present results.

The putative increased striatal cholinergic tone could activate ACh nicotinic and muscarinic receptors. The M2 and M4 receptors are good candidates to mediate this effect since they are both known to be expressed by these neurons and to be involved in modulation of ACh release (Bernard *et al.* 2006, Bernard *et al.* 1992, Zhang *et al.* 2002). The increased size of varicosities could also result from a trophic role of muscarinic receptors as previously reported (Di Liberto *et al.* 2017, Mount et al. 1994).

In addition to changes in the shape of neuronal varicosities in VAChT overexpressing mice, we found that varicosities display more mitochondria with increased size compared to WT animals. The distribution of mitochondria in neurons depends on the energy needed to accomplish specialized functions. Areas with high demands for ATP, such as axonal terminals, contain more mitochondria than other cellular domains (Brodin *et al.* 1999, Li *et al.* 2004, Nguyen *et al.* 1997). Moreover, the dynamics of mitochondria, including mitochondrial fission and fusion cycles, adapt the shape of mitochondria to the metabolic conditions of the

cell (Westermann 2012). Here, the presence of additional mitochondria supports the possibility that larger and less numerous CIN varicosities are more active.

It should be kept in mind that these large cholinergic varicosities could also be extrinsic to the striatum and originate from the brainstem (Dautan *et al.* 2016), as our experiments would be unable to differentiate varicosities from interneurons from those of projecting cholinergic neurons.

VAChT overexpression induces redistribution of VAChT in exo- and endocytotic pathways

To understand the trafficking of an overexpressed transporter in CIN and to identify how a putative cholinergic over-activity could modify the distribution of VAChT in CINs we identified which organelles expressed VAChT in CHAT-ChR2 mice. Our observations of VAChT accumulation in various exo- and endocytotic pathways suggest that, in ChAT-ChR2 mice, the excessive amounts of VAChT likely saturate each step normally used for its trafficking. Furthermore, our study suggests the pathways taken by the transporter between the cell body and varicosities in cholinergic neurons in vivo (see Fig. 7).

VAChT overexpression in the exocytotic pathway may result from activation of VAChT synthesis in the ER and maturation in the Golgi apparatus (as previously shown, (Kolisnyk et al. 2013)). Alternatively, we cannot exclude that the synthesis and maturation are normal. The excess of VAChT may thus be trapped in the ER and Golgi apparatus. This could be due to overwhelming saturation in the trafficking machinery required to direct proteins to post-synthesis compartments, including the plasma membrane, as previously reported for the muscarinic M2 receptor in a model of striatal cholinergic overactivity (Bernard et al. 2003, Bernard et al. 2006).

Our observation on VAChT distribution on the endocytic pathway (Figs 5 and 7) is in line with previous data describing endocytosis motifs in the cytoplasmic tail of VAChT that potentially interact with clathrin-associated protein adaptor protein 1 and 2 (Barbosa et al. 2002, Kim & Hersh 2004, Santos et al. 2001). According to our data, during its trafficking towards varicosities, VAChT could be directed first to the plasma membrane in cell bodies. Interestingly, VAChT contains a molecular motif involved in membrane addressing and in targeting to synaptic varicosities (Ferreira et al. 2005, Santos et al. 2001). In WT animals, VAChT is never co-detected with AChE, a membrane bound protein (Fig. 6d). Therefore, the presence of VAChT near the plasma membrane of perikarya in over-expressing mice may represent a very transient state in WT mice. At varicosities, EM experiments show that VAChT is often detected close to or at the plasma membrane. Due to the tiny shape of varicosities, it is hard to determine whether VAChT is associated with the membrane of with sub-membrane vesicles. The functional signification of the putative association of VAChT

with the plasma membrane is still unclear. This observation could reflect the increased activity of these enlarged terminals and in particular a jammed endocytic pathway.

The highest number and size of mitochondria shown in varicosities from VAChT overexpressing mice in our study suggests an overall activation of synaptic vesicle cycling and endocytosis. Indeed, the local demand in energy (and thus the number of mitochondria per terminals) likely correlates with the number of synaptic vesicles that undergo endocytosis (Marland *et al.* 2016).

The post-endocytic fate of VAChT may take different forms. VAChT may be degraded in lysosomes as suggested by co-localization of VAChT and cathepsin D. Alternatively, VAChT produced in perikarya may be transported along the axon towards varicosities and synaptic vesicle membrane (Fig. 7). This phenomenon called transcytosis has been reported for Trk receptors (Ascaño *et al.* 2009) but never for a vesicular transporter of neurotransmitter. Additional experiments are needed to test both hypotheses. Experiments using a pulse-chase approach may be necessary to confirm the proposed model. Time course to follow VAChT targeting will be needed to confirm the suggested model.

VAChT overexpression does not modify other markers of the cholinergic transmission

Our results show no modification of the overall expression of cholinergic markers. In the striatum, the major part of ChAT, AChE and CHT labeling is present in varicosities. Therefore, the absence of overall modification of cholinergic marker probably reflects that these markers are unchanged in varicosities. In addition, there is an increased colocalization of VAChT and cholinergic markers. This suggests a redistribution of these markers in the same subcellular compartments. Alternatively, it cannot be excluded that there is an increase of expression of these markers in the perikarya.

VAChT overexpression does not change drastically the localization of other pivotal markers of cholinergic transmission such as ChAT, AChE and CHT. Therefore, all morphological changes observed in these mice seems to be related to the excess of VAChT in CIN.

Conclusion

The present study describes morphological abnormalities of CIN and intraneuronal VAChT redistribution in VAChT overexpressing mice. These data allow us to propose a putative model of VAChT trafficking in CIN *in vivo* (Fig. 7). After synthesis and maturation, VAChT is targeted to the plasma membrane of the perikaryon. Then, VAChT undergoes endocytosis and is either sent to lysosomes to be degraded, or sent through the axon up to axonal varicosities. Taken together, our model is compatible with the trafficking process previously proposed in cultured cells overexpressing the transporter (Barbosa et al. 2002, Ferreira et al. 2005, Santos et al. 2001).

It is tempting to use ChAT-ChR2 mice to decipher the role of CIN in the regulation of striatal functions. However, it should be kept in mind that these mice display abnormal cholinergic neurotransmission and major morphological alterations that make them fundamental different from wild-type mice. Our work suggests the need for caution when using rodents in which ChAT- BAC transgenesis is used to regulate expression of proteins in cholinergic neurons.

Acknowledgements

This research was supported by funds from the *Fondation pour la Recherche Médicale* (*Équipe* FRM DEQ20130326486), the *Agence Nationale pour la Recherche* (ANR, ANR-13-SAMA-0005-01), the *Fédération pour la Recherche sur le Cerveau*, Labex (Bio-Psy Laboratory of Excellence), INSERM, CNRS and UPMC. M.A.M.P. and V.F.P. are supported by CIHR (MOP 126000, 136930, 89919), NSERC (402524-2013 RGPIN) and Brain Canada Multi-Investigator Research Initiative.

We are grateful to Odile Poirel for laboratory managing. We thank Susanne Bolte and Jean-François Gilles from the *Photon microscopy facility of the Institut de Biologie Paris-Seine* (Université Pierre et Marie Curie, Paris). We thank Michaël Trichet and Ghislaine Frébourg from the *Electron microscopy facility of the Institut de Biologie Paris-Seine* (Université Pierre et Marie Curie, Paris). We thank Ulf Schwartz from *Leica Microsystems (Mannheim, Germany)* for assistance with STED microscopy. We thank Sanda Raulic, Jue Fan, and Matthew Cowan for animal care and technical support.

Conflict of interest statement

Marco Prado is a handling editor for the Journal of Neurochemistry. The other authors have no conflict of interest.

Figure Legends

Figure 1

ChAT-ChR2 mice are more sensitive to low dose of cocaine in behavioral sensitization paradigm. Sensitivity to different doses of cocaine was tested in ChAT-ChR2 mice using behavioral sensitization paradigm. a : mice were injected with cocaine i.p. (10 mg/kg) for six successive days and distance travelled in the open field during the first 20 minutes after injection was analysed (n = 8 for both genotype). b and c : Mice were habituated to the open field and saline i.p. injections for three days. From the day 4, they received i.p. cocaine injection (10 or 20 mg/kg as indicated) and the distance travelled during first 30 minutes was recorded. After 5 days of withdrawal, locomotor response to cocaine was tested again on the day 13. Note that ranges of Y axes in a, b and c are set differently for better resolution, because the performance of WT mice differs depending on cocaine dose. Number of mice used are as follows: in b, n=4 (WT saline), n=10 (WT cocaine), n=4 (ChAT-ChR2 saline) and n=12 (ChAT-ChR2 cocaine); in c, n=5 (WT saline), n=10 (WT cocaine), n=5 (ChAT-ChR2 saline) and n=11 (ChAT-ChR2 cocaine). Significant differences between genotypes are indicated as **, $p < 0.05$ and ***, $p < 0.001$.

Figure 2

Immunohistochemical localization of VAChT and VGLUT3 in the striatum of WT and ChAT-ChR2 mice. Images were taken with a confocal (a-d') or a STED microscope (e-l). In the striatum of a WT (a, a') or a ChAT-ChR2 (b, b') mouse, VAChT is detected in the cytoplasm of a neuron (asterisk) and in axonal varicosities (arrows). In the striatum of a WT (c, c') or a ChAT-ChR2 (d, d') mouse, VGLUT3 is also detected in the cytoplasm of a neuron (asterisk) and in axonal varicosities (arrows). Note that the intensity of VAChT labeling is much increased in ChAT-ChR2 mice. In contrast, the intensity of VGLUT3 labeling is similar in WT and in ChAT-ChR2 mice. Using STED microscopy, at low magnification, VAChT is detected as spots of labeling (arrows in e) in a WT mouse. In a ChAT-ChR2 mouse, spots of labeling appear much larger (arrows in f). At higher magnification, VAChT immunostaining is observed as round-shaped spots within axonal varicosities in WT and ChAT-ChR2 mice. In WT mice, VAChT-positive spots entirely filled the varicosities (g-i). In ChAT-ChR2 mice VAChT labelling was located at the periphery of varicosities (j-l). Scale bars: a, b, c, d : 10µm; a', b', c', d', e, f : 5µm; e-j: 200nm.

Figure 3

Immunogold localization of VAChT in striatum of WT and ChAT-ChR2 mice at the electron microscopic level. a-d : Distribution of VAChT immunoparticles (IP) in the

perikaryon of WT and ChAT-CHR2 mice. In a WT animal, VAChT IP were detected mostly in the cytoplasm in association with endoplasmic reticulum (arrows) or Golgi apparatus (Go; a and c). In a perikaryon of ChAT-ChR2 mice, VAChT IP are abundantly detected in the cytoplasm in association with endoplasmic reticulum (b ; arrows), with large round-shaped compartments (inserts in b' and b'') and with Golgi apparatus (d ; Go). In WT mice, synaptic vesicles filled the varicosities (e, f). IP for VAChT were evenly distributed in the varicosity and some of them were seen in association with synaptic vesicles (arrow-heads). In varicosities from ChAT-ChR2 mice, synaptic vesicles were rarely identified (g-i, arrow-heads). VAChT IP were often located at or close to the plasma membrane. Sometimes, IP are associated with large round-shaped compartments (arrow in g). The surface of varicosities was larger in the striatum of ChAT-ChR2 mice (g-j) than in WT mice (e-f,j). The surface of mitochondria was also increased in varicosities of ChAT-ChR2 mice compared to those of WT animals (g-i,k). Quantification on EM images demonstrated that the size of varicosities and of the mitochondria in varicosities were significantly higher in ChAT-ChR2 mice compared to WT mice (surface of varicosities: +177%; surface of mitochondria : +93%; Mann Whitney U test : * : $p<0.01$; n=6 mice ; 20 varicosities/mouse ; 3 or 13 mitochondria/mouse in WT or ChAT-ChR2 animals). Scale bars : a-d: 500nm; b', b": 100nm; e-I : 200nm.

Figure 4

Immunohistochemical localization of VAChT in neuronal compartments involved in synthesis and maturation in the striatum of WT mice and ChAT-ChR2 mice. In WT animals (a,a',e,e',i,i'), VAChT colocalized rarely or never with PDI in the endoplasmic reticulum (a, arrow-head), TGN38 and GM130 in the Golgi apparatus of perikarya (e,i) or varicosities (insets, a',e',i'). In ChAT-ChR2 mice (b,f,j), VAChT was abundantly detected in the cytoplasma of perikarya. VAChT often colocalized with PDI, GM130 and TGN38 (arrows-heads. In axonal varicosities (insets, b',f',j') , VAChT colocalizes with all three markers (arrows-heads). The analysis of the colocalization of VAChT and PDI, GM130 and TGN38 in perikarya was performed using the Jacop pluggin of ImageJ and statistical data are reported from the Costes 's randomization-based colocalization module (see methods). For perikarya (c,g,k), data were expressed as a Pearson's coefficient (*pc*) and *pc* were compared using the Mann–Whitney U test. Our analysis has shown that the colocalization observed between the VAChT and immunofluorescent signal for organelle markers was not caused by chance coincidence in all WT and ChAT-ChR2 and for all combination of marker. Moreover, the colocalization of VAChT with PDI, GM130 and TGN38 (b,c,f,g,j,k, arrow-heads) is significantly higher in perikarya of ChAT-ChR2 mice compared to those from WT (Mann–Whitney U test: ***: $p<0.0001$). The Fisher's test demonstrated a highly significant increase in the proportion of varicosities expressing VAChT and PDI, GM130 and TGN38 (Fig. d,h,l;

*** : p<0.0001). Scale bars: a-f: 5µm; a'-f': 1µm.

Figure 5

Immunohistochemical localization of VAChT in neuronal compartments involved in endocytosis and degradation in the striatum of WT and ChAT-ChR2 mice.

In WT animals (a,a',e,e',i,i'), VAChT did not colocalize with CHC in clathrin-coated pits, Rab5 in early endosomes and Rab9 in late endosomes in perikarya (a,e,i) and varicosities (insets; a',e',i'). In ChAT-ChR2 mice (b,d,f), VAChT often colocalizes with CHC, Rab5 and Rab9 in perikarya (b,f,j) and in axonal varicosities (arrows-heads, b',f',j'). In WT animals (m, m'), VAChT did not colocalize with CathD in perikarya and varicosities (inset). In ChAT-ChR2 mice (n,n'), VAChT sometimes colocalized with CathD in perikarya (arrows-heads) and varicosities (inset, arrows-heads). The analysis of the colocalization of VAChT and CHC, Rab5, Rab9 and CathD in perikarya was performed using the Jacop pluggin of ImageJ and statistical data are reported from the Costes 's randomization-based colocalization module (see methods). For perikarya (c,g,k and o), data were expressed as a Pearson's coefficient (*pc*) and *pc* were compared using the Mann–Whitney U test. Our analysis has shown that the colocalization observed between the VAChT and immunofluorescent signal for organelle markers was not caused by chance coincidence in all WT and ChAT-ChR2 and for all combination of marker. Moreover, the colocalization of VAChT with CHC, Rab5, Rab9 and CathD (c,g,k and o) is significantly higher in perikarya of ChAT-ChR2 mice compared to those from WT (Mann–Whitney U test: ***: p<0.0001). The Fisher's test demonstrated a highly significant increase in the proportion of varicosities expressing VAChT and CHC, Rab5, Rab9 and CathD (Fig. d,h,l and p; *** : p<0.0001). Scale bars: a-h : 5µm; a'-h': 1µm.

Figure 6

Immunohistochemical detection of markers of the cholinergic system in CIN of WT and ChAT-ChR2 mice at confocal microscopic level.

ChAT, AChE, CHT were detected in the cytoplasm of perikarya of WT and ChAT-ChR2 mice (a-l). AChE was present at the plasma membrane (arrows, d and e). The analysis of the colocalization of VAChT and ChAT, AChE and CHT in perikarya was performed using the Jacop pluggin of ImageJ and statistical data are reported from the Costes 's randomization-based colocalization module (see methods). For perikarya (c,f,i and l), data were expressed as a Pearson's coefficient (*pc*) and *pc* were compared using the Mann–Whitney U test. Our analysis has shown that the colocalization observed between the VAChT and immunofluorescent signal for cholinergic markers was not caused by chance coincidence in all WT and ChAT-ChR2 and for all combination of marker. Moreover, the colocalization of VAChT with ChAT, AChE and CHT (b,c,e,f,h and i; arrow-heads) is significantly higher in

perikarya of ChAT-ChR2 mice compared to those from WT (Mann–Whitney U test: ***: $p<0.0001$). Scale bars: 1µm.

Figure 7

Schema proposed for VAChT trafficking in CIN in WT and ChAT-ChR2 mice.

This schema indicates progression of VAChT among the intracellular compartments suggested by these data. In WT mice, VAChT is mostly located at the level of axonal varicosities. VAChT follows synthesis and maturation and endocytotic pathways likely in a very transient way, before being transported to axonal varicosities. In ChAT-ChR2 mice, VAChT is abundantly present in the maturation and endocytotic compartments (endoplasmic reticulum and Golgi apparatus), then addressed to the plasma membrane from where it is internalized by clathrin-mediated endocytosis. Then VAChT would be either sent to lysosomes to be degraded, or transported up to axonal varicosities through a transcytotic mechanism.

References

Aran, A., Segel, R., Kaneshige, K. et al. (2017) Vesicular acetylcholine transporter defect underlies devastating congenital myasthenia syndrome. *Neurology,* **88,** 1021-1028.

Ascaño, M., Richmond, A., Borden, P. and Kuruvilla, R. (2009) Axonal targeting of Trk receptors via transcytosis regulates sensitivity to neurotrophin responses. *J Neurosci,* **29,** 11674-11685.

Barbosa, J., Ferreira, L. T., Martins-Silva, C. et al. (2002) Trafficking of the vesicular acetylcholine transporter in SN56 cells: a dynamin-sensitive step and interaction with the AP-2 adaptor complex. *J Neurochem,* **82,** 1221-1228.

Bernard, V., Brana, C., Liste, I., Lockridge, O. and Bloch, B. (2003) Dramatic depletion of cell surface m2 muscarinic receptor due to limited delivery from intracytoplasmic stores in neurons of acetylcholinesterase-deficient mice. *Mol Cell Neurosci,* **23,** 121-133.

Bernard, V., Décossas, M., Liste, I. and Bloch, B. (2006) Intraneuronal trafficking of G-protein-coupled receptors in vivo. *Trends Neurosci,* **29,** 140-147.

Bernard, V., Laribi, O., Levey, A. I. and Bloch, B. (1998) Subcellular Redistribution of m2 Muscarinic Acetylcholine Receptors in Striatal Interneurons In Vivo after Acute Cholinergic Stimulation. *J Neurosci,* **18,** 10207-10218.

Bernard, V., Levey, A. I. and Bloch, B. (1999) Regulation of the subcellular distribution of m4 muscarinic acetylcholine receptors in striatal neurons in vivo by the cholinergic environment: evidence for regulation of cell surface receptors by endogenous and exogenous stimulation. *J Neurosci,* **19,** 10237-10249.

Bernard, V., Normand, E. and Bloch, B. (1992) Phenotypical characterization of the rat striatal neurons expressing muscarinic receptor genes. *J Neurosci,* **12,** 3591-3600.

Bolte, S. and Cordelieres, F. P. (2006) A guided tour into subcellular colocalization analysis in light microscopy. *J Microsc,* **224,** 213-232.

Brodin, L., Bakeeva, L. and Shupliakov, O. (1999) Presynaptic mitochondria and the temporal pattern of neurotransmitter release. *Philos Trans R Soc Lond B Biol Sci,* **354,** 365-372.

Cervini, R., Houhou, L., Pradat, P. F., Béjanin, S., Mallet, J. and Berrard, S. (1995) Specific vesicular acetylcholine transporter promoters lie within the first intron of the rat choline acetyltransferase gene. *J Biol Chem,* **270,** 24654-24657.

Costes, S. V., Daelemans, D., Cho, E. H., Dobbin, Z., Pavlakis, G. and Lockett, S. (2004) Automatic and quantitative measurement of protein-protein colocalization in live cells. *Biophys J,* **86,** 3993-4003.

Crittenden, J. R., Lacey, C. J., Lee, T., Bowden, H. A. and Graybiel, A. M. (2014) Severe drug-induced repetitive behaviors and striatal overexpression of VAChT in ChAT-ChR2-EYFP BAC transgenic mice. *Front Neural Circuits,* **8,** 57.

Dautan, D., Hacioglu Bay, H., Bolam, J. P., Gerdjikov, T. V. and Mena-Segovia, J. (2016) Extrinsic Sources of Cholinergic Innervation of the Striatal Complex: A Whole-Brain Mapping Analysis. *Front Neuroanat,* **10,** 1.

Deisseroth, K. (2015) Optogenetics: 10 years of microbial opsins in neuroscience. *Nat Neurosci,* **18,** 1213-1225.

Di Chiara, G., Morelli, M. and Consolo, S. (1994) Modulatory functions of neurotransmitters in the striatum: ACh/dopamine/NMDA interactions. *Trends Neurosci,* **17,** 228-233.

Di Liberto, V., Borroto-Escuela, D., Frinchi, M., Verdi, V., Fuxe, K., Belluardo, N. and Mudò, G. (2017) Existence of muscarinic acetylcholine receptor (mAChR) and fibroblast growth factor receptor (FGFR) heteroreceptor complexes and their enhancement of neurite outgrowth. *Biochim Biophys Acta,* **1861,** 235-245.

Dobbertin, A., Hrabovska, A., Dembele, K., Camp, S., Taylor, P., Krejci, E. and Bernard, V. (2009) Targeting of acetylcholinesterase in neurons in vivo: a dual processing function for the proline-rich membrane anchor subunit and the attachment domain on the catalytic subunit. *J Neurosci,* **29,** 4519-4530.

Eiden, L. E. (1998) The cholinergic gene locus. *J Neurochem,* **70,** 2227-2240.

El Mestikawy, S., Wallen-Mackenzie, A., Fortin, G. M., Descarries, L. and Trudeau, L. E. (2011) From glutamate co-release to vesicular synergy: vesicular glutamate transporters. *Nat Rev Neurosci,* **12,** 204-216.

Erickson, J. D., Varoqui, H., Schäfer, M. K. et al. (1994) Functional identification of a vesicular acetylcholine transporter and its expression from a "cholinergic" gene locus. *J Biol Chem,* **269,** 21929-21932.

Faul, F., Erdfelder, E., Buchner, A. and Lang, A. G. (2009) Statistical power analyses using G*Power 3.1: tests for correlation and regression analyses. *Behav Res Methods,* **41,** 1149-1160.

Fei, H., Grygoruk, A., Brooks, E. S., Chen, A. and Krantz, D. E. (2008) Trafficking of vesicular neurotransmitter transporters. *Traffic,* **9,** 1425-1436.

Ferguson, S. M., Savchenko, V., Apparsundaram, S., Zwick, M., Wright, J., Heilman, C. J., Yi, H., Levey, A. I. and Blakely, R. D. (2003) Vesicular localization and activity-dependent trafficking of presynaptic choline transporters. *J Neurosci,* **23,** 9697-9709.

Ferreira, L. T., Santos, M. S., Kolmakova, N. G. et al. (2005) Structural requirements for steady-state localization of the vesicular acetylcholine transporter. *J Neurochem,* **94,** 957-969.

Fiszman, M. L., Barberis, A., Lu, C., Fu, Z., Erdelyi, F., Szabo, G. and Vicini, S. (2005) NMDA receptors increase the size of GABAergic terminals and enhance GABA release. *J Neurosci,* **25,** 2024-2031.

Fiszman, M. L., Erdelyi, F., Szabo, G. and Vicini, S. (2007) Presynaptic AMPA and kainate receptors increase the size of GABAergic terminals and enhance GABA release. *Neuropharmacology,* **52,** 1631-1640.

Gonzales, K. K. and Smith, Y. (2015) Cholinergic interneurons in the dorsal and ventral striatum: anatomical and functional considerations in normal and diseased conditions. *Ann N Y Acad Sci,* **1349,** 1-45.

Gras, C., Amilhon, B., Lepicard, E. M. et al. (2008) The vesicular glutamate transporter VGLUT3 synergizes striatal acetylcholine tone. *Nat Neurosci,* **11,** 292-300.

Gras, C., Herzog, E., Bellenchi, G. C., Bernard, V., Ravassard, P., Pohl, M., Gasnier, B., Giros, B. and El Mestikawy, S. (2002) A third vesicular glutamate transporter expressed by cholinergic and serotoninergic neurons. *J Neurosci,* **22,** 5442-5451.

Guzman, M. S., De Jaeger, X., Raulic, S. et al. (2011) Elimination of the vesicular acetylcholine transporter in the striatum reveals regulation of behaviour by cholinergic-glutamatergic co-transmission. *PLoS Biol,* **9,** e1001194.

Hikida, T., Kitabatake, Y., Pastan, I. and Nakanishi, S. (2003) Acetylcholine enhancement in the nucleus accumbens prevents addictive behaviors of cocaine and morphine. *Proc Natl Acad Sci U S A,* **100,** 6169-6173.

Kilkenny, C., Browne, W., Cuthill, I. C., Emerson, M., Altman, D. G. and Group, N. C. R. R. G. W. (2010) Animal research: reporting in vivo experiments: the ARRIVE guidelines. *J Gene Med,* **12,** 561-563.

Kim, M. H. and Hersh, L. B. (2004) The vesicular acetylcholine transporter interacts with clathrin-associated adaptor complexes AP-1 and AP-2. *J Biol Chem,* **279,** 12580-12587.

Kitabatake, Y., Hikida, T., Watanabe, D., Pastan, I. and Nakanishi, S. (2003) Impairment of reward-related learning by cholinergic cell ablation in the striatum. *Proc Natl Acad Sci U S A,* **100,** 7965-7970.

Kolisnyk, B., Al-Onaizi, M. A., Xu, J., Parfitt, G. M., Ostapchenko, V. G., Hanin, G., Soreq, H., Prado, M. A. and Prado, V. F. (2016) Cholinergic Regulation of hnRNPA2/B1 Translation by M1 Muscarinic Receptors. *J Neurosci,* **36,** 6287-6296.

Kolisnyk, B., Guzman, M. S., Raulic, S., Fan, J., Magalhaes, A. C., Feng, G., Gros, R., Prado, V. F. and Prado, M. A. (2013) ChAT-ChR2-EYFP mice have enhanced motor endurance but show deficits in attention and several additional cognitive domains. *J Neurosci,* **33,** 10427-10438.

Krantz, D. E., Waites, C., Oorschot, V., Liu, Y., Wilson, R. I., Tan, P. K., Klumperman, J. and Edwards, R. H. (2000) A phosphorylation site regulates sorting of the vesicular acetylcholine transporter to dense core vesicles. *J Cell Biol,* **149,** 379-396.

Kreitzer, A. C. and Berke, J. D. (2011) Investigating striatal function through cell-type-specific manipulations. *Neuroscience,* **198,** 19-26.

Li, Z., Okamoto, K., Hayashi, Y. and Sheng, M. (2004) The importance of dendritic mitochondria in the morphogenesis and plasticity of spines and synapses. *Cell,* **119,** 873-887.

Lim, S. A., Kang, U. J. and McGehee, D. S. (2014) Striatal cholinergic interneuron regulation and circuit effects. *Front Synaptic Neurosci,* **6,** 22.

Lima Rde, F., Prado, V. F., Prado, M. A. and Kushmerick, C. (2010) Quantal release of acetylcholine in mice with reduced levels of the vesicular acetylcholine transporter. *J Neurochem,* **113,** 943-951.

Marland, J. R., Hasel, P., Bonnycastle, K. and Cousin, M. A. (2016) Mitochondrial Calcium Uptake Modulates Synaptic Vesicle Endocytosis in Central Nerve Terminals. *J Biol Chem,* **291,** 2080-2086.

Martyn, A. C., De Jaeger, X., Magalhaes, A. C. et al. (2012) Elimination of the vesicular acetylcholine transporter in the forebrain causes hyperactivity and deficits in spatial memory and long-term potentiation. *Proc Natl Acad Sci U S A,* **109,** 17651-17656.

Mount, H. T., Dreyfus, C. F. and Black, I. B. (1994) Muscarinic stimulation promotes cultured Purkinje cell survival: a role for acetylcholine in cerebellar development? *J Neurochem,* **63,** 2065-2073.

Nagy, P. M. and Aubert, I. (2012) Overexpression of the vesicular acetylcholine transporter increased acetylcholine release in the hippocampus. *Neuroscience,* **218,** 1-11.

Nguyen, P. V., Marin, L. and Atwood, H. L. (1997) Synaptic physiology and mitochondrial function in crayfish tonic and phasic motor neurons. *J Neurophysiol,* **78,** 281-294.

O'Grady, G. L., Verschuuren, C., Yuen, M. et al. (2016) Variants in SLC18A3, vesicular acetylcholine transporter, cause congenital myasthenic syndrome. *Neurology,* **87,** 1442-1448.

Pothos, E. N., Larsen, K. E., Krantz, D. E., Liu, Y., Haycock, J. W., Setlik, W., Gershon, M. D., Edwards, R. H. and Sulzer, D. (2000) Synaptic vesicle transporter expression regulates vesicle phenotype and quantal size. *J Neurosci,* **20,** 7297-7306.

Prado, V. F., Martins-Silva, C., de Castro, B. M. et al. (2006) Mice deficient for the vesicular acetylcholine transporter are myasthenic and have deficits in object and social recognition. *Neuron,* **51,** 601-612.

Prado, V. F., Roy, A., Kolisnyk, B., Gros, R. and Prado, M. A. (2013) Regulation of cholinergic activity by the vesicular acetylcholine transporter. *Biochem J,* **450,** 265-274.

Ray, A., Liu, J., Karanth, S., Gao, Y., Brimijoin, S. and Pope, C. (2009) Cholinesterase inhibition and acetylcholine accumulation following intracerebral administration of paraoxon in rats. *Toxicol Appl Pharmacol,* **236,** 341-347.

Ren, J., Qin, C., Hu, F., Tan, J., Qiu, L., Zhao, S., Feng, G. and Luo, M. (2011) Habenula "cholinergic" neurons co-release glutamate and acetylcholine and activate postsynaptic neurons via distinct transmission modes. *Neuron,* **69,** 445-452.

Ribeiro, F. M., Alves-Silva, J., Volknandt, W. et al. (2003) The hemicholinium-3 sensitive high affinity choline transporter is internalized by clathrin-mediated endocytosis and is present in endosomes and synaptic vesicles. *J Neurochem,* **87,** 136-146.

Roghani, A., Feldman, J., Kohan, S. A., Shirzadi, A., Gundersen, C. B., Brecha, N. and Edwards, R. H. (1994) Molecular cloning of a putative vesicular transporter for acetylcholine. *Proc Natl Acad Sci U S A,* **91,** 10620-10624.

Roy, A., Fields, W. C., Rocha-Resende, C., Resende, R. R., Guatimosim, S., Prado, V. F., Gros, R. and Prado, M. A. (2013) Cardiomyocyte-secreted acetylcholine is required for maintenance of homeostasis in the heart. *FASEB J,* **27,** 5072-5082.

Sakae, D. Y., Marti, F., Lecca, S. et al. (2015) The absence of VGLUT3 predisposes to cocaine abuse by increasing dopamine and glutamate signaling in the nucleus accumbens. *Mol Psychiatry,* **20,** 1448-1459.

Santos, M. S., Barbosa, J., Veloso, G. S., Ribeiro, F., Kushmerick, C., Gomez, M. V., Ferguson, S. S., Prado, V. F. and Prado, M. A. (2001) Trafficking of green fluorescent protein tagged-vesicular acetylcholine transporter to varicosities in a cholinergic cell line. *J Neurochem,* **78,** 1104-1113.

Santos, M. S., Li, H. and Voglmaier, S. M. (2009) Synaptic vesicle protein trafficking at the glutamate synapse. *Neuroscience,* **158,** 189-203.

Steidl, S., Wang, H., Ordonez, M., Zhang, S. and Morales, M. (2016) Optogenetic excitation in the ventral tegmental area of glutamatergic or cholinergic inputs from the laterodorsal tegmental area drives reward. *Eur J Neurosci*.

Steketee, J. D. and Kalivas, P.W. (2011) Drug wanting: behavioral sensitization and relapse to drug-seeking behavior. *Pharmacol Rev.* **63**, 348-365.

Sugita, S., Fleming, L. L., Wood, C. et al. (2016) VAChT overexpression increases acetylcholine at the synaptic cleft and accelerates aging of neuromuscular junctions. *Skelet Muscle,* **6,** 31.

Tan, P. K., Waites, C., Liu, Y., Krantz, D. E. and Edwards, R. H. (1998) A leucine-based motif mediates the endocytosis of vesicular monoamine and acetylcholine transporters. *J Biol Chem,* **273,** 17351-17360.

Ting, J. T. and Feng, G. (2014) Recombineering strategies for developing next generation BAC transgenic tools for optogenetics and beyond. *Front Behav Neurosci,* **8,** 111.

Wang, L., Zhang, X., Xu, H. et al. (2014) Temporal components of cholinergic terminal to dopaminergic terminal transmission in dorsal striatum slices of mice. *J Physiol,* **592,** 3559-3576.

Westermann, B. (2012) Bioenergetic role of mitochondrial fusion and fission. *Biochim Biophys Acta,* **1817,** 1833-1838.

Williams, M. J. and Adinoff, B. (2008) The role of acetylcholine in cocaine addiction. *Neuropsychopharmacology,* **33,** 1779-1797.

Yao, J. and Hersh, L. B. (2007) The vesicular monoamine transporter 2 contains trafficking signals in both its N-glycosylation and C-terminal domains. *J Neurochem,* **100,** 1387-1396.

Zhang, W., Yamada, M., Gomeza, J., Basile, A. S. and Wess, J. (2002) Multiple muscarinic acetylcholine receptor subtypes modulate striatal dopamine release, as studied with M1-M5 muscarinic receptor knock-out mice. *J Neurosci,* **22,** 6347-6352.

Zhao, S., Ting, J. T., Atallah, H. E. et al. (2011) Cell type-specific channelrhodopsin-2 transgenic mice for optogenetic dissection of neural circuitry function. *Nat Methods,* **8,** 745-752.

Zhao, Y. and Keen, J. H. (2008) Gyrating clathrin: highly dynamic clathrin structures involved in rapid receptor recycling. *Traffic,* **9,** 2253-2264.

Ztaou, S., Maurice, N., Camon, J., Guiraudie-Capraz, G., Kerkerian-Le Goff, L., Beurrier, C., Liberge, M. and Amalric, M. (2016) Involvement of Striatal Cholinergic Interneurons and M1 and M4 Muscarinic Receptors in Motor Symptoms of Parkinson's Disease. *J Neurosci,* **36,** 9161-9172.

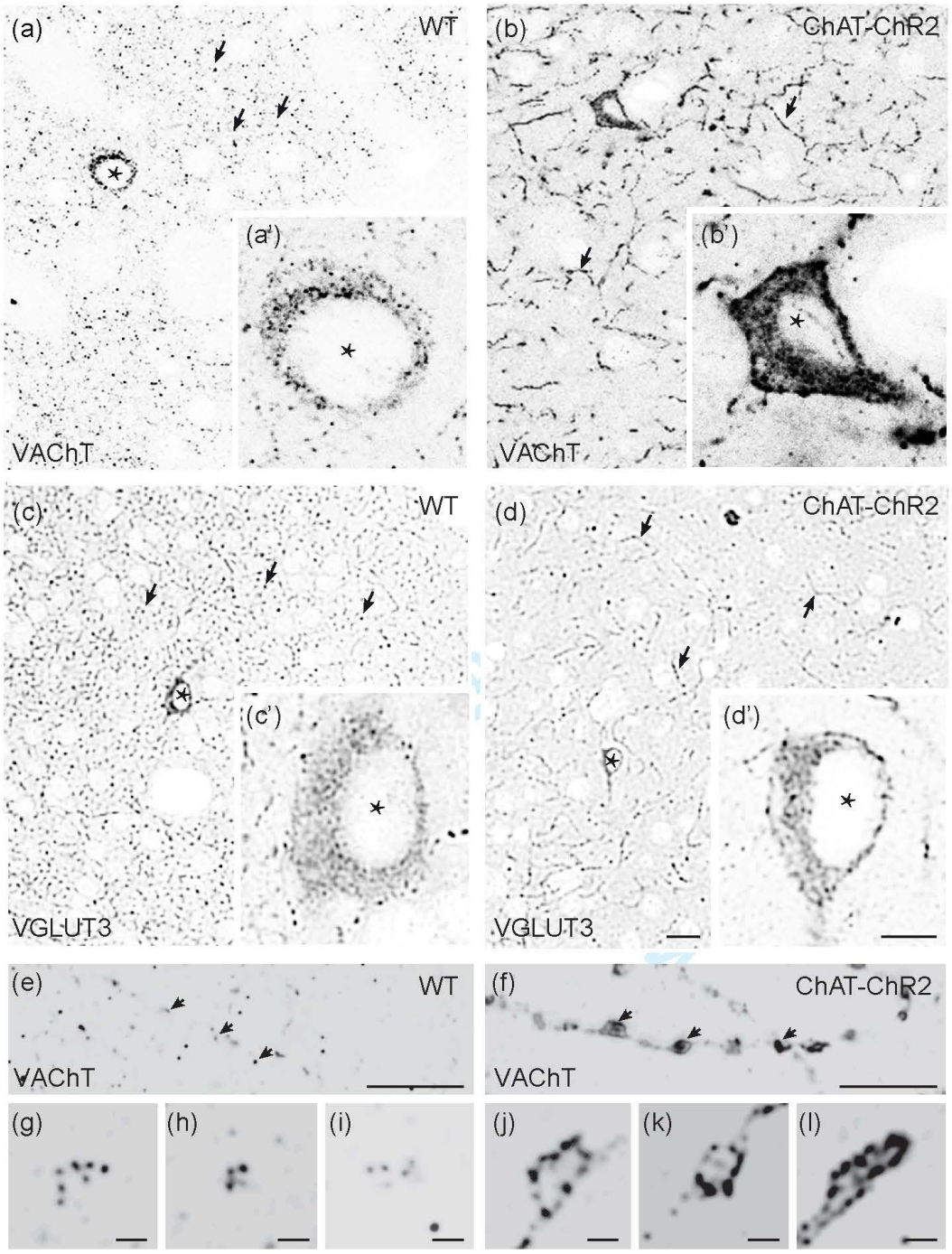

Figure 2 Janickova et al.

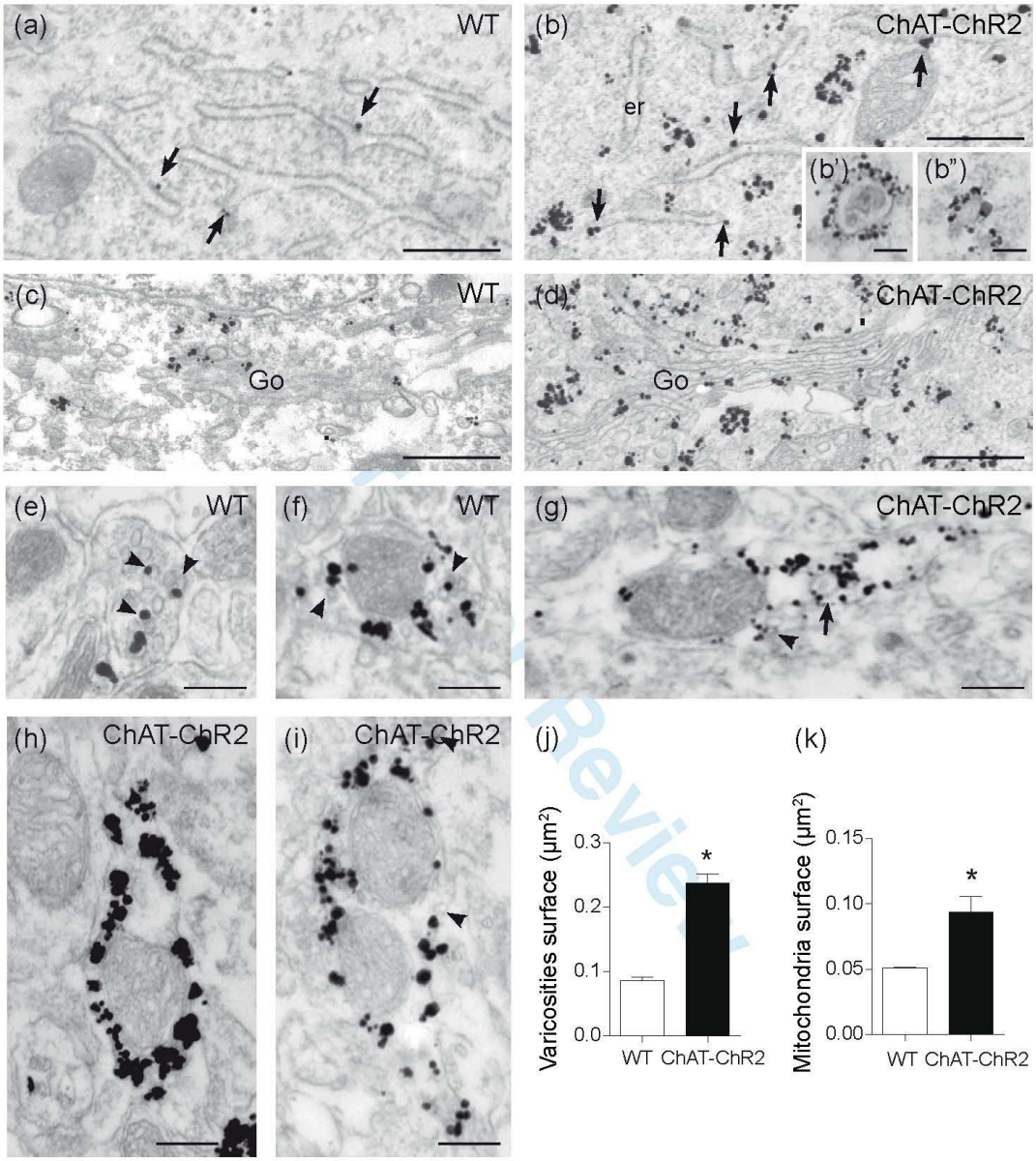

Figure 3 Janickova et al.

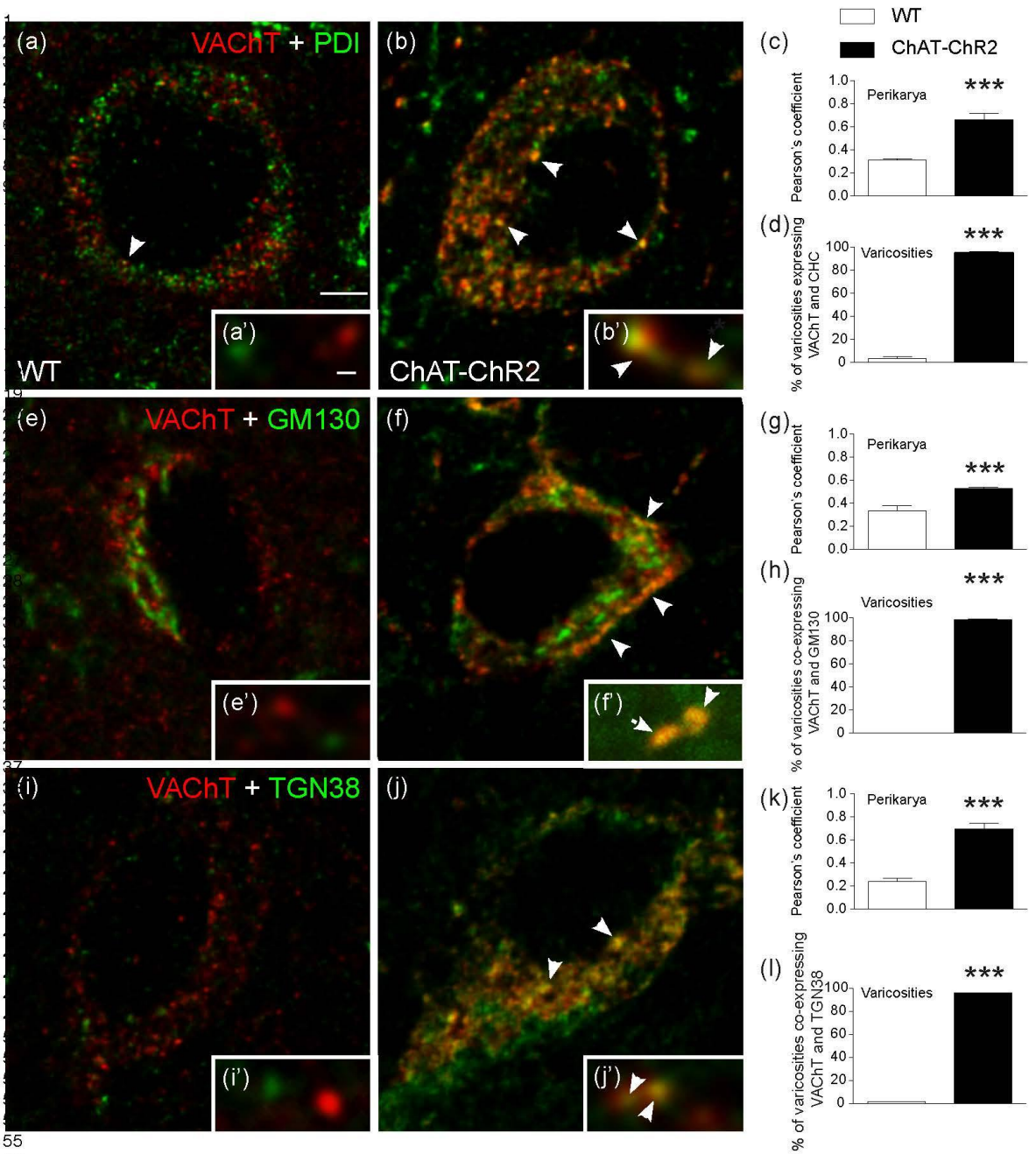

Figure 4 Janickova et al.

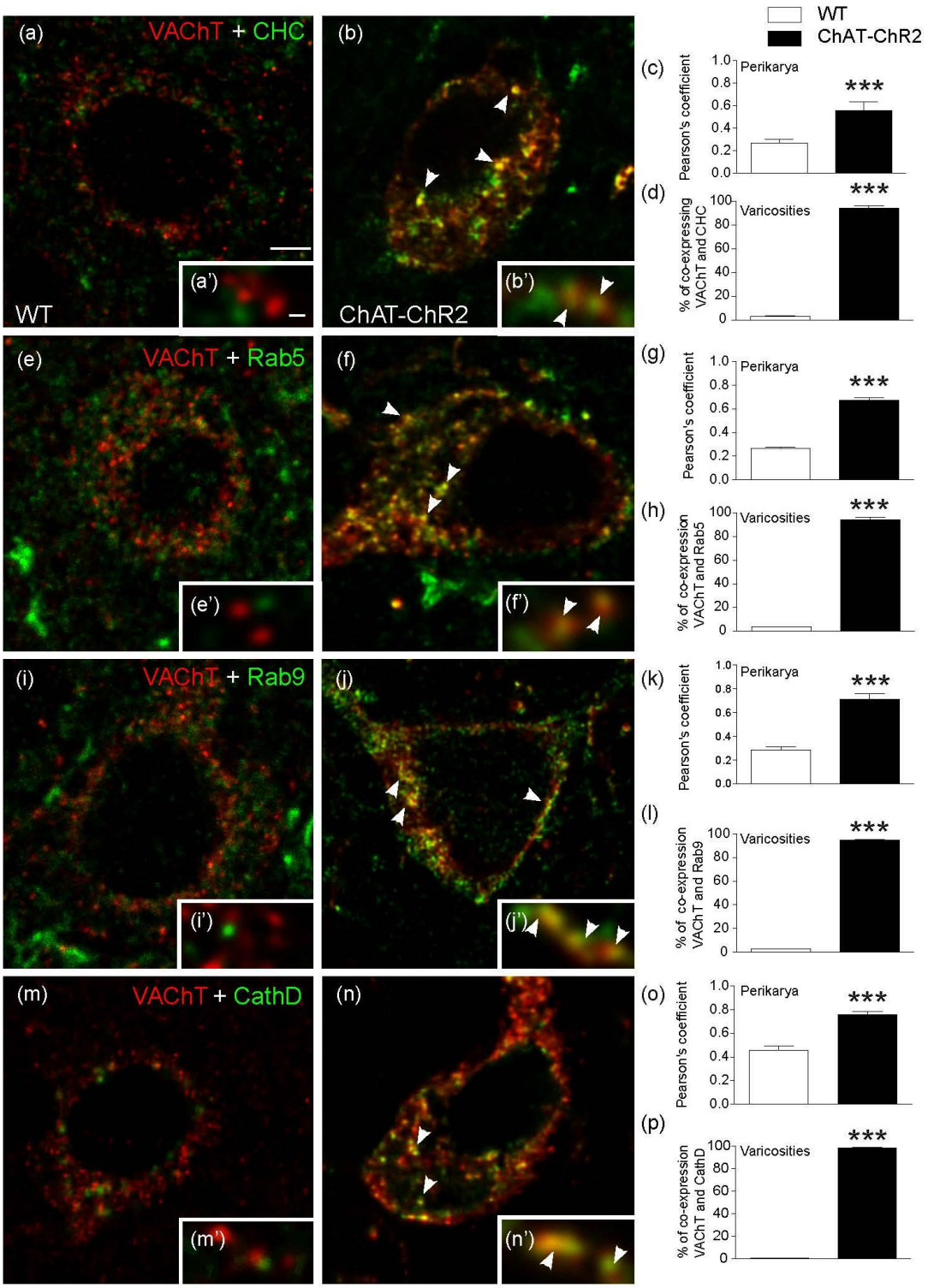

Figure 5 Janickova et al.

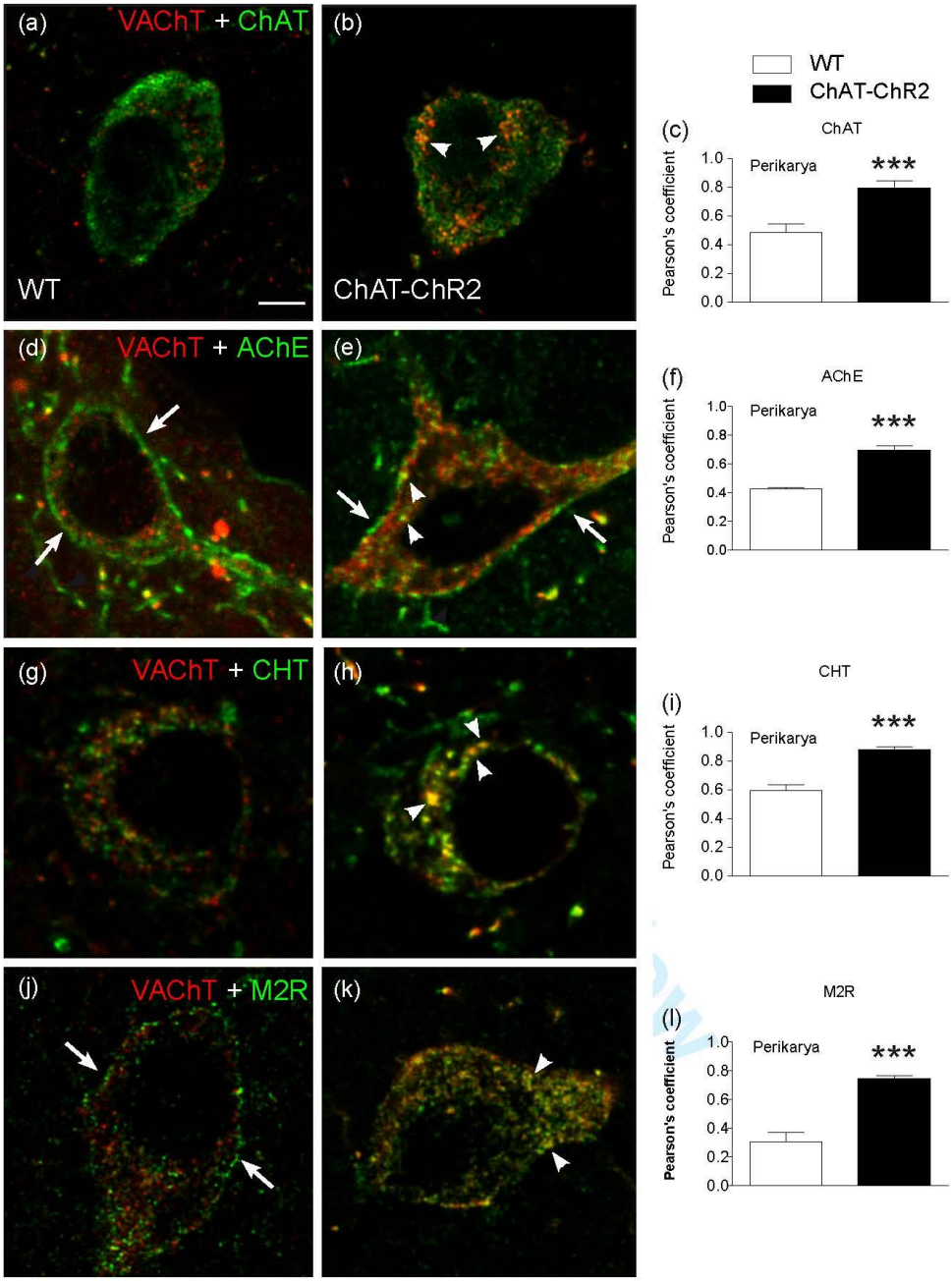

Figure 6 Janickova et al.

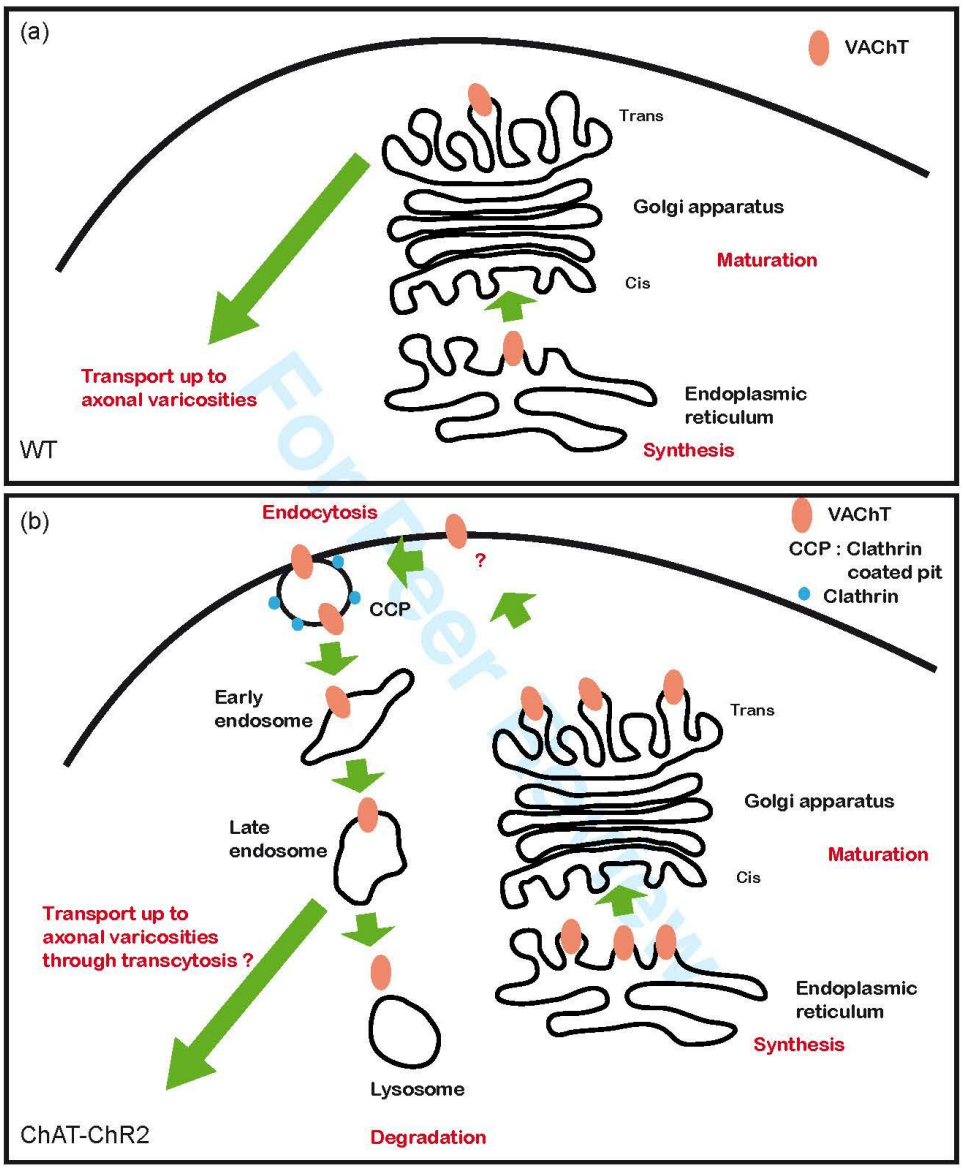

Figure 7 Janickova et al.

Supporting Information

Title : Vesicular Acetylcholine Transporter (VAChT) overexpression induces major modifications of striatal cholinergic interneuron morphology and function

Helena Janickova[1], Vania F. Prado[1], Marco A.M. Prado[1], Salah El Mestikawy[2,3] and Véronique Bernard[2*]

[1]Robarts Research Institute, Molecular Medicine Laboratories, Department of Physiology and Pharmacology and Department of Anatomy & Cell Biology, The University of Western Ontario, Molecular Medicine, 1151 Richmond St. N, N6A 5B7, London, Ontario, Canada; [2]Sorbonne Universités, Université Pierre et Marie Curie UM 119 - CNRS UMR 8246 - INSERM U1130, Neurosciences Paris Seine - Institut de Biologie Paris Seine (NPS - IBPS), 75005 Paris, France,
[3]Douglas Mental Health University Institute, Department of Psychiatry, McGill University, Montreal, Canada.

* **Corresponding author** : Véronique Bernard, Neuroscience Paris Seine, Sorbonne Universités, Université Pierre et Marie Curie UM 119 - CNRS UMR 8246 - INSERM U1130, Bât B 4ème étage pièce 425, 9 quai Saint Bernard, case courrier 37, 75005, Paris, France,
Tel: +33 6 10 09 68 93; Fax: +33 1 44 27 60 69.
veronique.bernard@inserm.fr

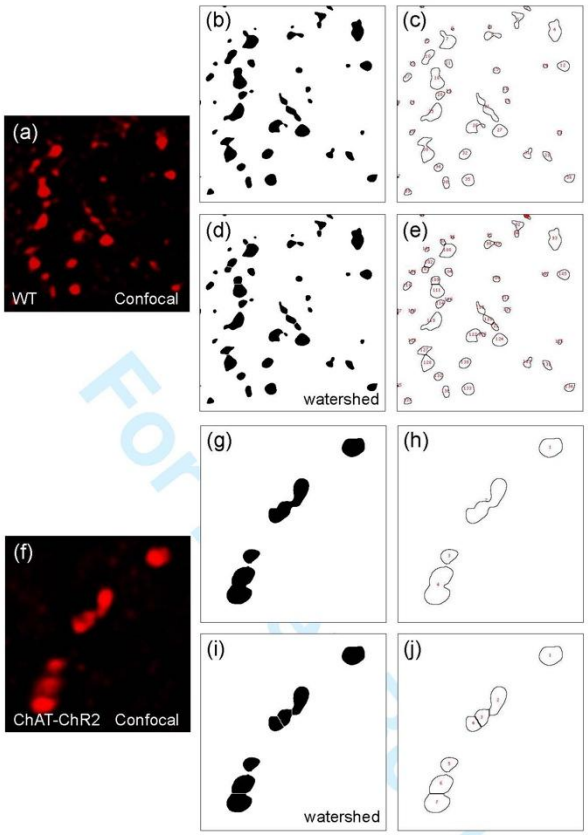

Figure S1

Method of counting of the density of VAChT immunopositive varicosities using the watershed segmentation.

Striatal sections labeled for VAChT immunoreactivity were observed using the x63 objective and acquisitions were performed under the confocal microscope. Labeling was then analyzed using the ImageJ software. Because there is overstaining for VAChT in the BAC mice, it could be that the individual puncta visible in the control mice are overlapping in the BAC mice leading to lower quantal counts only because they cannot be resolved. To correct this bias, we have analyzed our pictures using a method that allow to separate touching fluorescent objects. This method, called the watershed separation, is performed with the ImageJ software. Briefly, after thresholding, the varicosities are separated from the background (b,g). Then, the varicosities are separated one from another, with the watershed function (1d,i) and counted with the analyze particles function (1e,j). The density of spots corresponds to the number of spots divided by the surface of the fields (655µm^2).

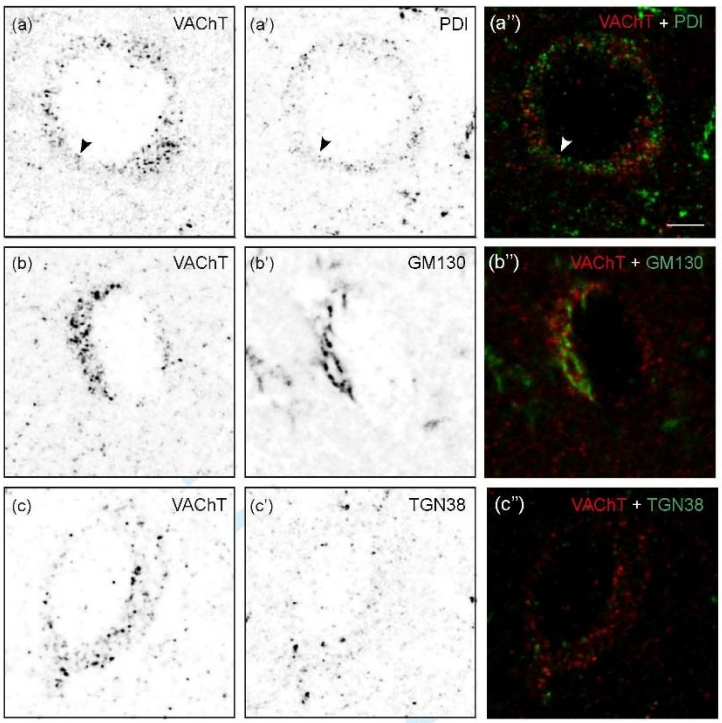

Figure S2

Colocalization of VAChT in neuronal compartments involved in synthesis and maturation in CIN perikarya of the striatum of WT mice.

We show here the individual channels first before the overlay is presented in order to get an unbiased impression of potential co-labeling. The first channel shows VAChT labeling (a-c) and the second one presents PDI (a'), GM130 (b') and TGN38 (c') staining. Pannels a'', b'' and c'' correspond to the overlay. Almost no detectable colocalization of VAChT with PDI, GM130 and TGN38 was seen with PDI, GM130 and TGN38 (arrows-heads). Scale bars: a-c'' : 5µm.

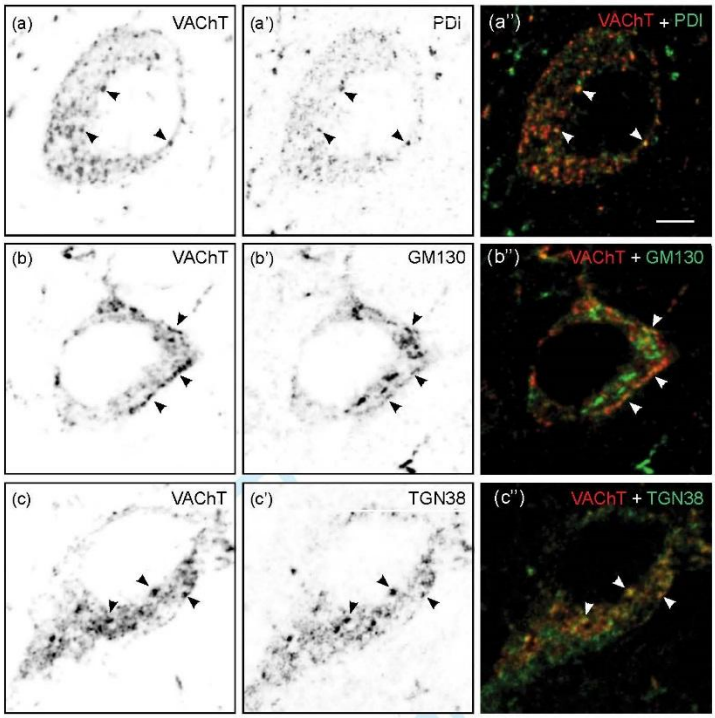

Figure S3

Colocalization of VAChT in neuronal compartments involved in synthesis and maturation in CIN perikarya of the striatum of ChAT-ChR2 mice.

We show here the individual channels first before the overlay is presented in order to get an unbiased impression of potential co-labeling. The first channel shows VAChT labeling (a-c) and the second one presents PDI (a'),GM130 (b') and TGN38 (c') staining. Pannels a'', b'' and c'' correspond to the overlay. VAChT often colocalized with PDI, GM130 and TGN38 (arrows-heads). Scale bars: a-c'' : 5µm.

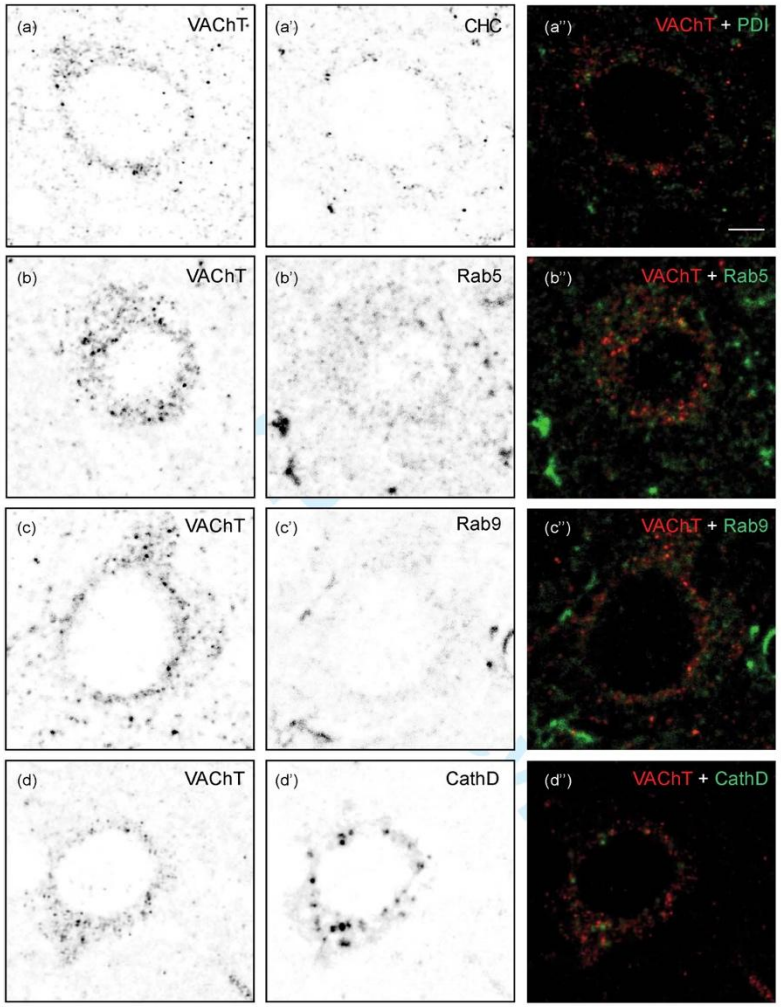

Figure S4

Colocalization of VAChT in neuronal compartments involved in endocytosis and degradation in CIN perikarya of the striatum of WT mice.

We show here the individual channels first before the overlay is presented in order to get an unbiased impression of potential co-labeling. The first channel shows VAChT labeling (a-d) and the second one presents CHC (a'), Rab5 (b'), Rab9 (c') and CathD (d') staining. No detectable colocalization of VAChT with PDI, GM130 and TGN38 was seen (arrows-heads). Pannels a'', b'', c'' and d'' correspond to the overlay. Scale bars: a-d'' : 5µm.

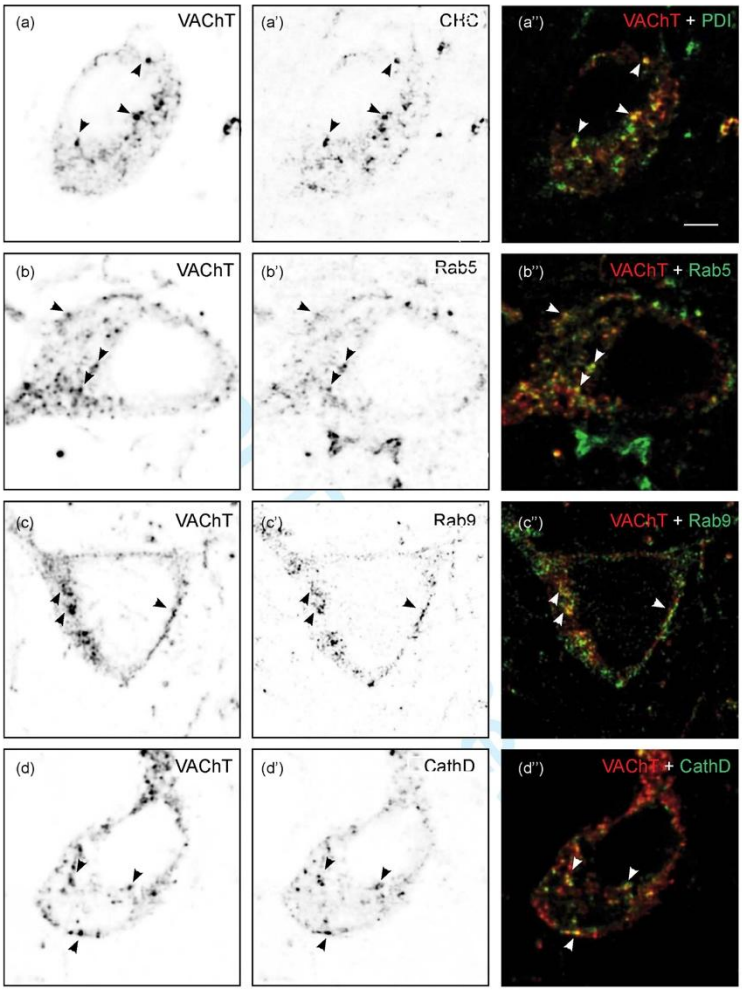

Figure S5

Colocalization of VAChT in neuronal compartments involved in endocytosis and degradation in CIN perikarya of the striatum of ChAT-ChR2 mice.

We show here the individual channels first before the overlay is presented in order to get an unbiased impression of potential co-labeling. The first channel shows VAChT labeling (a-d) and the second one presents CHC (a'), Rab5 (b'), Rab9 (c') and CathD (d') staining. VAChT often colocalized with PDI, GM130 and TGN38 (arrows-heads). Pannels a'', b'', c'' and d'' correspond to the overlay. Scale bars: a-d'' : 5µm.